Chimeric CNS-Targeting-Peptide Engineered Exosomes for Experimental Allergic Encephalomyelitis Therapy

Yingkai Wang
Guangxi University https://orcid.org/0000-0002-2867-9508
Yunpeng Zhao
Naval Medical University
Mingzhu Ye
Zhongshan Hospital Xiamen University
Ling Wang
Naval Medical University
Tianshu Lan
Xiamen Medical College
Yue Wang
Naval Medical University
Zhongquan Qi (yxyyz@gxu.edu.cn)
Guangxi University https://orcid.org/0000-0002-7210-4955

Research

Keywords: nanotherapeutics, exosomes, mesenchymal stem cells, multiple sclerosis, regulatory T cells, T cells, experimental autoimmune encephalomyelitis

Posted Date: November 3rd, 2021

DOI: https://doi.org/10.21203/rs.3.rs-1007673/v1

Abstract

Background: Multiple sclerosis (MS), an inflammatory disease of the central nervous system (CNS), leads to demyelination, neuronal injury, and loss of white matter, yet still can't be cured. Exosomes are double-layered membrane vesicles of 30–200 nm in size, which can easily penetrate the blood–brain barrier (BBB). Exosomes derived from umbilical cord mesenchymal stem cells exosomes (UMSC-exos) has been shown to treat experimental autoimmune encephalomyelitis (EAE) through the action of anti-inflammatory and immunomodulatory, but its clinical translation has been hampered by their inefficacious accumulation in CNS. Therefore, we developed a TAxI-peptide-chimeric UMSC-exos termed TAxI-exos for CNS-specific accumulation and curative effect in EAE.

Methods: We used an EAE model in vivo, and actived T cells and BV-2 cells models in vitro. After two immunizations to establish the EAE model, UMSC-exos, TAxI-exos or DiR labeled exosomes were administered to EAE mice EAE mice for one dose (150μg) before the peak at day 15. On day 30, the mice were sacrificed to collect spinal cords, spleens, and blood for analysis of demyelination, inflammation, microglia, the proportions of T-cell subsets, and the expression of inflammatory cytokines. In vitro, for immune mechanism analyses, PBMCs and splenocytes isolated from healthy C57BL/6 mice, were activated and incubated with 0.15mg/mL UMSC-exos or TAxI-exos. Activated BV-2 cells were used to explore the targeting-ability and polarization-regulating ability of UMSC-exos and TAxI-exos.

Results: As expected, TAxI-exos had significant curative effects in EAE mice compared with UMSC-exos via an enhanced targeting-ability. The treatment alleviated inflammation, facilitated microglial cell polarization from M1 to M2, reduced the proportions of T-cell subsets, increased the expression levels of IL-4, IL-10, TGF-β, and IDO-1, and decreased the levels of IL-2, IL-6, IL-17A, IFN-γ, and TNF-α.

Conclusions: TAxI-exos have a great CNS-targeting ability and suppress pathological processes in EAE mice, which have a great potential therapeutic utility for MS and other CNS diseases.

Background

MS is an autoimmune disease of the central nervous system (CNS), which leads to demyelination, neuronal injury, loss of white matter, and eventually leaves patients permanently disabled and blind, who are always young women [1]. More than 2 million people suffer from MS worldwide, with approximately 30 thousand patients in China [2]. Currently, 19 disease-modifying therapies (DMTs) have been approved for treatment of MS [3]. However, they are only effective for some patients in relapsing remitting multiple sclerosis (RRMS) [4], and only one drug was recently approved for secondary progressive multiple sclerosis (SPMS). Additionally, long-term treatment leads to tolerance, and increasing the types and dosages of medicines [5]. Therefore, it is critical to develop a novel and effective therapeutic drug.

The experimental autoimmune encephalomyelitis (EAE) is one of the most ideal animal models in MS research. The clinicopathological features of the model are similar to MS patients [6]. At the onset of MS and EAE, inflammatory cells infiltrate in brain and spinal cord tissues, and release cytokines along with

damaging of the BBB [7]. T helper (Th) 1 cells [8] and Th17 cells [9] play the main roles in the initiation of EAE. When IL-6 and IFN-γ are locally present, naive CD4+ T cells are selectively induced to differentiate into Th1 and Th17 cells [10] to activate macrophages/microglia, which contributes to cellular immunity by secreting IFN-γ, IL-2, TNF-α, and IL17A [11]. An M1/M2 microglial cell polarization imbalance is also a critical cellular mechanism of MS pathogenesis. M1 microglia produce pro-inflammatory cytokines (TNF-α and IL-6) to accelerate the EAE course, while M2 microglia have an anti-inflammatory effect [12].

Mesenchymal stem cells (MSCs) are a type of highly proliferative multipotent cells that can be isolated from various tissues, have a great potential in the fields of biotherapy, immunoregulation and tissue regeneration [13]. At early stages of EAE, an underlying mechanism is the ability of MSCs to induce a $CD4^+CD25^+Foxp3^+$ regulatory T cells (Tregs) population and suppress the differentiation processes of Th1 and Th17 cells [14]. MSCs exosomes, a type of lipid bilayer membrane vesicles, with a diameter of 50–200 nm, harbor many bioactive factors such as proteins, lipids, and microRNAs secreted from their parent cells [15]. Because of their excellent BBB-penetrating ability, humoral stability, and low immunogenicity compared with parent stem cells, umbilical cord MSCs exosomes (UMSC-exos) have become a treatment option for EAE. However, many studies have confirmed that intravenously injected exosomes are mainly distributed in the liver or spleen, and have very low tropism to other organs, even the CNS in EAE [16]. Thus, how to enhance the CNS-targeting ability of UMSC-exos is required before using UMSC-exos for MS therapy.

The SACQSQSQMRCGGG peptide (targeted axonal import, TAxI) is a novel targeting ligand with high affinity for axons, which delivers functional proteins to spinal cord motor neurons after peripheral administration [17]. Accordingly, we developed CNS-targeting TAxI-exos by modifying UMSC-exos with the TAxI peptides for MS therapy. In this study, we assessed the therapeutic effects of TAxI-exos and UMSC-exos in EAE mice by evaluating differences in the targeting ability, clinical symptoms, histology, microglial polarization, proportions of T cell subsets, and expression levels of inflammatory factors. Furthermore, we investigated the underlying mechanisms of these effects.

Methods

EAE induction and exosomes treatment

8 to10-week-old female C57BL/6 mice (18-22 g) were purchased from Wu's Experimental Animals Inc. (Shanghai, China). Animals were cared in accordance with the guidelines of the Animal Ethics Committee of Xiamen Medical College (Approval ID: 20190302007).

To induce EAE, female C57BL/6J mice were immunized with 200 μg MOG35–55 (Sinobioway Co., Ltd., Zhangzhou, China) in complete Freund's adjuvant (Chondrex Inc., WA, USA) with 4 mg/mL heated-killed *M. Tuberculosis* (H37Ra, non-viable). Pertussis toxin (List Biological Laboratories Inc., CA, USA) was intraperitoneally injected at 400 ng on days 0 and 2. After 15-20 days, mice displayed the peak of the disease showing complete paralysis of the tail and hind limbs.

UMSC-exos or TAxI-exos (150 μg or 2×10^{10} particles) was intravenously injected (i.v.) once before the peak of the disease. Each mouse was assessed daily by a clinical score that ranged from 0 to 5 [18]: No clinical disorder in motor functions compared with non-immunized mice (0); partial tail weakness or slight loss of muscle tone (0.5); limp tail (1.0); limp tail and hind legs paralysis with gait abnormality (2.0); limp tail and complete paralysis of hind legs (3.0); limp tail and complete paralysis of hind legs and partial front leg paralysis (3.5); front and hind limb paralysis (4.0); moribund state (5.0). Mice were monitored for at least 30 days after immunization.

Cells

Human umbilical cords were provided by Zhongshan Hospital affiliated to Xiamen University as the source of human umbilical cord tissue-derived MSCs (UC-MSCs) and UMSC-exos used in this study. UC-MSCs were isolated from discarded umbilical cords and prepared by following an established protocol [19].

The cells were fully characterized following an established protocol [20]. They expressed specific cell surface markers CD44, CD73, CD81, CD105, and CD90 and did not express negative marker HLA-DR (PeproTech Inc., NJ, USA) in vitro. For exosome collection, 80% confluent cells were cultured in complete media (Meilunbio, Dalian, China) supplemented without fetal bovine serum (FBS) for 48h.

For in vitro experiments, microglial cell line BV-2 was cultured in DMEM-high glucose (Meilunbio) supplemented with 10% FBS. The cells were incubated at 37 °C in a humidified atmosphere with 5% CO_2.

Isolation of exosomes

As described above, conditioned medium from cultures of UC-MSCs was collected and centrifuged at 300 × *g* for 10 min and then 2000 × *g* for 20 min at 4 °C to remove cell debris pellet and larger vesicles. Supernatants were transferred to centrifuge bottles (Centrifuge bottles polypropylene with caps 29 × 104 mm, Beckman Coulter, CA, USA) and centrifuged in a high speed refrigerated centrifuge (Avanti JXN-26 centrifuge, Beckman Coulter) for 20 min at 12,000 × *g* at 4 °C (Type JA-25.50 rotor, Beckman Coulter), to remove microvesicles. The supernatants were filtered through a 0.22-μm filter (Millipore, MA, USA) and then carefully collected in 40 PA tubes (26 × 90 mm, TKY, Japan) and ultracentrifuged for 1.5 h in a Type R30AT rotor at 110,000 × *g* at 4 °C (High-speed refrigerated centrifuge CR30NX, Himac). The exosomes (UMSC-exos) were reconstituted in PBS and stored at −80 °C. For experiments, exosomes prepared from three different UC-MSCs batches were pooled to reduce any potential effect of batch-to-batch variations on molecular markers.

Preparation of axon-targeted exosomes

Targeting ligands was incorporated into UMSC-exos by a post-insertion method mediated by DSPE-PEG2000 in accordance with a previous study [21].

Briefly,1,2-distearoyl-sn-glycero-3-phosphoethanolamine-N-[methoxy(polyethylene glycol)-2000]-KSACQSQSQMRCGGGK-Biotin (DSPE-PEG2000-TAxI, Ruixi, Xi'an, China) was dissolved in 4-(2-hydroxyethyl)-1-piperazineethanesulfonic acid buffer for 10 min at 60 °C to form micelles. Then, the UMSC-exos suspension was mixed with the above suspension and ultrasonicated at 15% AMPL for 5min (VCX150, Sonics & Materials Inc., Leics, UK), prior to incubation for 2 h at 40 °C. After cooling to room temperature (RT), the mixture was immediately purified by 300K ultrafiltration centrifuge tube (Pall, NYC, USA) to get TAxI-exos. Then, purified TAxI-exos were analyzed by NTA and TEM.

Electron microscopy

UMSCs exosomes were analyzed under a transmission electron microscope (TEM) (HT7700 Exalen, Hitachi, TKY, Japan) by following previously published protocol [22].

Nanoparticle tracking analysis (NTA)

NTA was performed using a nanoparticle tracking analyzer (ZetaView PMX120, Particle Metrix, Bavaria Germany). UMSC-exos and TAxI-exos suspended in PBS were diluted 1000-fold prior to analysis. The precise diameter of exosomes were characterized by NTA that tracks the particle movement to obtain size information. A 60-s video was recorded and subsequently analyzed using NTA software.

Internalization of UMSC-exos or TAxI-exos with BV-2 in vitro

UMSC-exos and TAxI-exos were labeled with the 1,1'-dioctadecyl-3,3,3',3-tetramethylindocarbocyanine iodide (DiR, Useverbright® Inc., Suzhou, China) according to the manufacturer's instructions. For fluorescence microscopy, BV-2 cells were labeled with 5,6-carboxyfluorescein diacetate, succinimidyl ester (CFDA SE, Yeasen, Shanghai, China) according to the manufacturer's instructions and then exposed to the DiR-labeled exosomes (0.4mg/ml or 5×10^{10} particles mL^{-1}) for 12 h in Glass Bottom Cell Culture Dish (Φ15 mm, NEST, Wuxi, China). The samples was examined under a fluorescence microscope (Leica Microsystems, Wetzlar, Germany) and analyzed using ImageJ-Fiji (NIH, MD, USA).

Biodistribution of exosomes in vivo

Wild-type (WT) and EAE mice were used to access the biodistribution of DiR labeled UMSC-exos or TAxI-exos. Mice (n = 3) were intravenously administered with 150 μg (or 2×10^{10} particles) DiR-labeled UMSC-exos or TAxI-exos. Fluorescence images of the mouse body were recorded and analyzed by the IVIS® Lumina XRMS III and analysis software (Perkin-Elmer, MD, USA) at 24 and 48 h after injection.

Histopathological examination

For immunohistochemical staining, at the time of sacrifice, 4% paraformaldehyde-fixed spinal cords were removed and cut into 4 μm thick sections. At least six sections were examined for each mouse. The sections were incubated with a primary antibody against Iba-1 (1:200 dilution; Huabio, Hangzhou, China) at 4 °C overnight. Then, the samples were incubated with a secondary antibodies (HRP conjugated goat

anti-rabbit IgG, 1:500 dilution; Servicebio, Wuhan, China) for 1 h at RT. The sections were observed under an Axio Imager (Zeiss, Aalen, Germany). Quantification of Iba-1 staining was performed in three sections each from three mice of one group using ImageJ-Fiji IHC Toolbox plugins (The University of Nottingham, UK).

Luxol fast blue (LFB, Leagene®, China) staining determines myelin differentiation. Spinal cord sections went through a series of staining steps in accordance with the manufacturer's instructions. Quantification of myelinated axon areas was performed using three sections each from three mice of one group. All spinal cord sections were observed under the Axio Imager (Zeiss) and analyzed using ImageJ-Fiji.

For hematoxylin and eosin staining, spinal cord sections were stained and went through a series of ethanol washes, and analyzed under the Axio Imager (Zeiss). Inflammatory cell infiltration was scored as follows [12]: no infiltrating cells = 0; a few scattered infiltrating cells = 1; organization of inflammatory cell infiltration around blood vessels = 2; extensive perivascular cuffing with widespread cell infiltration = 3.

Protein quantification

Exosomes were diluted in PBS and were analyzed using a microBCA protein assay kit (Sangon, Shanghai, China). Tissues and cells were lysed in cold RIPA buffer (Meilunbio) with a protease inhibitor cocktail (Meilunbio). After centrifugation at 4 °C for 10 min, supernatant was collected and subjected to quantification using a BCA protein assay kit (Solarbio, Beijing, China) and western blot. The plate was analyzed using a SpectraMax i3x and software (Molecular Devices, SV, USA).

Western blot (WB)

Prepare UMSC-exos, UMSCs, or spinal cord proteins with volumes corresponding to twenty μg protein were used for analysis. The following antibodies were used: primary antibodies Calnexin (1:1000), TSG101 (1:2000), CD9 (1:1000), CD63 (1:1000), CD81 (1:1000), MBP (1:100) (Affinity Biosciences,OH, USA), iNOS (1:500), Arg-1 (1:1000) (Huabio); secondary antibodies Rabbit anti-mouse IgG (Huabio). Finally the washed membranes were incubated with Fg super sensitive ECL luminescent reagent (Affinity) and analyzed using a Chemidoc MP (Bio-Rad Laboratories, CA, USA).

Flow cytometry (FCM)

UMSCs were harvested from culture plates and washed with 1% BSA in PBS. MSCs were then incubated with PE-labeled antibodies against CD73, CD90, or CD105, an APC-labeled anti-CD44, and FITC-labeled anti-HLA-DR or an isotype as the control (BioGems, PeproTech) for 40 min at 4 °C. The samples were analyzed using a CytoFLEX LX (Beckman Coulter). Data were processed using FlowJo Software v.10 (Tri Star, Ashland, OR, USA).

For flow cytometry, the cells isolated from spleens or spinal cords of mice were washed with PBS. Cells were suspended and filtered through a 200-mesh sieve, prior to centrifuging at 500 × *g* for 5 min to collect. Peripheral blood mononuclear cells (PBMCs) were isolated from blood using a Mouse Peripheral

Lymphocyte Separation Kit (Meilunbio) for medium density gradient centrifugation and stained for markers of T cell subsets. The following antibodies were used: anti-IL-17-PE, anti-IFN-γ-PE, anti-CD4-FITC, anti-CD25-PE, anti-Foxp3-APC or an isotype as control (eBioscience, CA, USA).

T-cell proliferation assay

PBMCs were isolated from blood samples of healthy female mice using density gradient centrifugation. Thirty micrograms UMSC-exos or TAXI-exos were incubated with 1×10^5 CFDA SE labeled PBMCs. To stimulate T-cell proliferation, anti-mouse SAFIRE Purified CD3 (6 μg/mL) and CD28 (3μg/mL) (PeproTech) were used. After 4 days, cells were analyzed using flow cytometry. Data were analyzed using FlowJo V.10. The culture medium was stored at -80°C for cytokine measurements.

Treg induction assay

Splenocytes from healthy female mice were filtered through a 200-mesh sieve, and then centrifugated at 500 × *g* for 5 min. Suspensions were prepared and stimulated with anti-mouse CD3 SAFIRE Purified (3 μg/mL) and murine recombination IL-2 (30 ng/mL). The splenocytes further cultured with UMSC-exos or TAXI-exos (30 μg/well) or unconditioned medium as the control. Tregs are marked by expression of FOXP3 and high level of CD25 [23]. After 3 days, cells were stained for analysis of $CD4^+CD25^+FOXP3^+$ T cells by flow cytometry using the CytoFLEX LX and FlowJo V10.

Cytokine measurements

For serum samples, ELISAs for TGF-β (Cat#: EMC107b, Neobiocisence, China) and IL-1β (Cat#: EK201BHS, Multisciences, China*)* were performed in accordance with the manufacturers' protocols.

For the cytometric bead array (CBA) assay, 50 μL of PBMC culture supernatant or 10 μL of a mouse serum sample were incubated with 50 μL assay beads and 50 μL of reagent using a CBA Mouse Th1/Th2/Th17 Cytokine Kit (Cat No. 560485, BD, USA). Results were analyzed with FCAP Array Software (BD) and then reported as the mean fluorescence intensity (MFI).

Quantitative reverse transcription-PCR (qRT-PCR)

Total RNA was isolated from spinal cord (lumber enlargement) tissue using Column Animal RNAOUT reagent (Tiandz, Beijing, China) in accordance with the manufacturer's instructions. Reverse transcription of total RNA to cDNA and quantitative real-time PCR were performed using a One Step qRT-PCR SYBR Green Kit (Vazyme, Nanjing, China). The primers (Invitrogen, Suzhou, China) are listed in **Table 1**. The results were analyzed by the $2-\Delta\Delta Ct$ method and represented as fold changes, normalized to GAPDH.

Table. 1 Sequences of primers used for qPCR.

Gene	Gene bank accession		Sequence
GAPDH	NM_008084.2	Forward	5'- AGGTCGGTGTGAACGGATTTG -3'
		Reverse	5'- GGGGTCGTTGATGGCAACA-3'
IL-6	NM_031168.2	Forward	5'-TGGGACTGATGCTGGTGACA-3'
		Reverse	5’-ACAGGTCTGTTGGGAGTGGT-3’
IL-10	NM_010548.2	Forward	5’- CGGGAAGACAATAACTGCACCC -3’
		Reverse	5’- CGGTTAGCAGTATGTTGTCCAGC -3’
TNF-α	NM_013693.3	Forward	5'- GCCTCTTCTCATTCCTGCTTGTGG -3'
		Reverse	5'- GTGGTTTGTGAGTGTGAGGGTCTG -3'
IDO1	NM_008324.2	Forward	5'-CCTGCAATCAAAGCAATCC-3'
		Reverse	5'-CCACAAAGTCACGCATCCT-3'

Statistical analysis

Each experiment was repeated at least three times. All data were represented as the mean ± SEM using GraphPad Prism 5 software (GraphPad Inc., USA). Comparisons of two groups were performed by the *t*-test. One-way ANOVA with Bonferroni’s or Newman-Keuls post-hoc tests were applied to compare multiple groups. *p*-values of less than 0.05 were considered statistically significant.

Results

Identification of UMSCs

Before subcultured UMSCs were used in experiments, they were confirmed by MSCs standards [24]. When primary cells had migrated from umbilical cord tissues and adhered to the bottom of the culture flask, UMSCs gradually began to display a fibroblast-like and spindle-shaped morphology, which gathered together in a circinate appearance, as observed under an inverted phase contrast microscope (**Fig. 1a**). Surface markers on P3–P5 UMSCs were detected by FCM, which were positive for CD44, CD73, CD81, CD90, and CD105, but negative for HLA-DR (**Fig. 1b**). The purity of MSCs was up to 95% and no obvious morphological changes were observed.

Isolation and identification of UMSC-exos

A large number of UMSCs were cultured in medium without FBS for 48 h. Next, we purified exosomes from culture supernatants using differential centrifugation [25]. Exosome pellets were reconstituted in PBS and stored at −80 °C before use. Isolated UMSC-exos were characterized by WB, TEM, and NTA. CD9, CD63, CD81 and TSG101 were enriched in UMSC-exos, which was confirmed by WB **(Fig. 1c)**. An absence of Calnexin (endoplasmic reticulum marker) suggested that there was no contamination from

endoplasmic reticulum-derived vesicles **(Fig. 1c)**. TEM showed that UMSC-exos had a spherical shape and bilayer membrane structure with a diameter of approximately 130 nm (**Fig. 1d**). Furthermore, the precise sizes of exosomes were characterized by NTA. A screenshot of the NTA video is presented in **Figure 1e**. The average size of exosomes was determined to be approximately 116.6 nm in diameter **(Fig. 1f)**. Taken together, these data demonstrated successful isolation of UMSC-exos that expressed several common exosomal markers.

Preparation of TAxI-exos

TAxI peptides as drug delivery motors carry protein drugs aimed at axons [17]. First, we synthesized TAxI (SACQSQSQMRCGGG) peptides. Then, TAxI peptide was attached to DSPE-PEG2000-NHS to obtain DSPE-PEG2000-TAxI.

TAxI peptides were identified quantitatively and qualitatively by high performance liquid chromatography and mass spectroscopy. The purity was 95.05% and the molecular weight was 1880.2 (**Fig. 2a, b**). The structures of DSPE-PEG2000-TAxI were identified by infrared spectroscopy and the nuclear magnetic resonance (**Fig. 2c, d**).

To obtain applicative TAxI-exos, UMSC-exos were modified with DSPE-PEG2000-TAxI by a post-insertion method, which were named TAxI-exos (**Fig. 2e**). The morphology of UMSC-exos and TAxI-exos were assessed by TEM. They were both round spherical vesicles and TAxI-exos had a larger particle diameter than UMSC-exos (**Fig. 2f**). The average diameters and concentrations of UMSC-exos and TAxI-exos were analyzed by NTA, which were 138.4 and 150.6 nm (**Fig. 2g)**. These results indicated that UMSC-exos maintained integrity after the TAxI modification and had a larger particle diameter because of the TAxI peptides insertion.

Targeting capabilities of UMSC-exos and TAxI-exos in vivo and in vitro

After preparation of TAxI-exos, we confirmed the targeting ability of TAxI-exos in vivo. First, female C57BL/6 mice were immunized twice on days 0 and 2, and approximately 15~20 days later, EAE mice displayed the peak of the disease, which showed complete paralysis of the tail and hind limbs with a flattened posture. Next, each mouse was assigned a clinical score every day, which ranged from 0 to 5 in the monitoring stage (**Fig. 3a**). UMSC-exos and TAxI-exos were labeled with DiR. Then, 150 μg (or 2×10^{10} particles) DiR-labeled UMSC-exos or TAxI-exos were injected (i.v.) into EAE mice at day 15 ($n = 3$). The intensity of fluorescence signals was recorded at 24 and 48 h by a live imaging system (**Fig. 3b)**. The results show that the fluorescence intensity in the brain region of TAxI-exo-treated mice was significantly higher than that after UMSC-exos treatment and DiR-labeled UMSC-exos could not be detected after 24 or 48 h **(Fig. 3c)**. In the TAxI-exos group, no significant difference was observed in the fluorescence intensity between 24 and 48 h, which was the same in the UMSC-exos group **(Fig. 3c)**. Additionally, in EAE animals, the fluorescence intensity in the TAxI-exo-treated group had a slightly stronger trend, whereas in WT animals, this trend was weakened between 24 and 48 h **(Fig. 3c)**. These results suggested that TAxI peptides enhanced the blood stability and target-site residential capability of UMSC-exos.

Next, we assessed the internalization ability of TAxI-exos in target cells of the CNS in vitro. To this end, we chose BV-2 cells for CFDA SE staining and incubated with 0.4mg/mL (or 5×10^{10} particles mL^{-1}) DiR-labeled UMSC-exos or TAxI-exos and then the fluorescence signal was observed under a fluorescence microscope (**Fig. 3d**). Stronger signals occurred in BV-2 cells incubated with TAxI-exos than in those with UMSC-exos (**Fig. 3e**), which suggested that TAxI-exos had a significant BV-2 cell-targeting ability in vitro.

In this study, we applied in vitro and in vivo models to specifically demonstrate the CNS-targeting properties of TAxI-exos that accumulated in CNS sites more efficiently than UMSC-exos.

UMSC-exos and TAxI-exos improve clinical functional signs in EAE

We next examined the therapeutic effects of UMSC-exos and TAxI-exos in a well-established EAE model. To determine whether UMSC-exos and TAxI-exos could alleviated clinical symptoms associated with EAE, clinical scores and body weight measurements were recorded after EAE induction and exosomes treatments. Higher clinical scores and lower weights indicated deterioration of motor dysfunction and increased disease severity.

UMSC-exos and TAxI-exos were injected (i.v.) schematically (**Figure 3a)**. A single injection dose of UMSC-exos or TAxI-exos approximately 150 μg (or 2×10^{10} particles) per mouse was used before the disease peak (day 12-18), data were collected, and then the mice were sacrificed at day 30 (**Fig. 4a**). UMSC-exos and TAxI-exos treatment respectively resulted in mean clinical scores of 1.44 ± 0.13 and 1.0 ± 0.10 at day 30. Additionally, TAxI-exo-treated mice showed a significant improvement ($p < 0.001$) compared with EAE mice (mean clinical score of 2.03 ± 0.29) ($n = 5$) (**Fig. 4b**). UMSC-exos ($n = 5$) also ameliorated the disease, but to a lesser extent than TAxI-exos (mean body weight of 19.53 ± 0.47, $p < 0.001$) with a body weight of 16.53 ± 1.37 ($p < 0.01$) compared with EAE mice (n=5, mean clinical score of 2.03 ± 0.29) (**Fig. 4c**). These data verified that UMSC-exos and TAxI-exos effectively reduced the severity of EAE in mice.

UMSC-exos and TAxI-exos alleviate demyelination in EAE mice

Clinical symptoms in EAE mice are associated with demyelination in the spinal cord [7]. Therefore, we analyzed the severity of demyelination in spinal cord from each experimental group of mice.

Spinal cord sections of variously treated mice were analyzed for myelin by LFB staining **(Fig. 5a)**. Spinal cord sections from UMSC-exo- and TAxI-exo-treated mice ($n = 3$; > 6 sections per animal) both showed reductions in the degree of demyelination ($n = 3$; 40.44% ± 9.64%; $p < 0.01$) ($n = 3$; 20.07% ± 5.60%; $p < 0.001$) compared with EAE mice ($n = 3$; 57.22% ± 2.36%) and the former had a lesser extent than the latte **(Fig. 5b)**.

The levels of MBP (a structural protein of myelin) in spinal cords from TAxI-exo- and UMSC-exo-treated EAE mice were analyzed by WB **(Fig. 5c)**. Similarly, the results showed that both TAxI-exos and UMSC-exos had significantly increased the expression of MBP compared with the EAE group **(Fig. 5d)**.

These results suggested that TAxI-exos and UMSC-exos alleviated demyelination associated with the progression of EAE.

UMSC-exos and TAxI-exos modulate microglia polarization in vitro and in vivo

Because an M1/M2 phenotype imbalance is considered to initiate EAE, we verified the mechanism of UMSC-exos and TAxI-exos in microglia polarization in vitro. UMSC-exos or TAxI-exos were applied to BV-2 cells. Lipopolysaccharide (LPS) was added to simulate an inflammatory microenvironment for BV-2, and PBS treatment was used as a control. After 24 h, we observed BV2 cell morphology under a microscope. Cells in the PBS group were approximately oval or diamond in shape with small bodies. In the LPS group, cells had become ramified and swollen after stimulation **(Fig. 6a)**. Subsequently, the expression levels of CD86 and CD206 were evaluated to determine the M1/M2 phenotype **(Fig. 6b)**. Compared with the control group (n=3, 35.67% ± 0.61%), the LPS group had an increased density of $CD86^+$ cells that co-expressed CD206 (n=3, 80.93% ± 2.96%, $p < 0.001$), which was inhibited by UMSC-exos (n=3,48.10%±0.30%, $p < 0.001$) and TAxI-exos (n=3, 19.87% ± 0.62%, $p < 0.001$) **(Fig. 6c)**. A significant increase of $CD206^+$ cells was observed after TAxI-exos treatment (n=3, from 5.57% ± 0.38% to 1.84% ± 0.29% in the LPS group, $p < 0.05$) **(Fig. 6c)** and decreases of $CD86^+$ cells were induced by UMSC-exos (n=3, 1.02% ± 0.01% , $p < 0.01$) and TAxI-exos (n=3, 1.50% ± 0.15% , $p < 0.05$) compared with the LPS group (n=3, 6.70% ± 2.60%) **(Fig. 6c)**.

In vivo, WB was used to detect expressions of M1 and M2 phenotype-associated soluble markers in spinal cords of each group of mice **(Fig. 6d, e)**. The level of M1 phenotypic marker iNOS was significantly decreased in both UMSC-exo- and TAxI-exo-treated group (n=3) **(Fig. 6f)**, while the level of M2 phenotypic marker Arg-1 was increased significantly **(Fig. 6g)** compared with the EAE group. Additionally, the expression level of Iba-1 (a Ca^{2+}-binding protein indicative of macrophages and microglia) was evaluated in gray matter areas of immunohistochemically stained spinal cord sections **(Fig. 6h)**. The results of AOD analysis (IOD/area), indicated that TAxI-exo- (n = 3, 0.07 ± 0.01, $p < 0.001$) and UMSC-exo-treated mice (n=3, 0.08 ± 0.01 , p < 0.001) showed significant decreases in macrophage/microglia infiltration compared with the EAE group (n = 3, 0.29 ± 0.01) **(Fig. 6i)**.

These results suggested that UMSC-exos and TAxI-exos treatments not only significantly inhibited the conversion of microglia to the M1 phenotype and promoted polarization to the M2 phenotype in vitro, but also decreased macrophage/microglia infiltration in mouse spinal cords.

UMSC-exos and TAxI-exos display T cells suppressive activities both in vitro and in vivo

To confirm whether UMSC-exos and TAxI-exos suppressed T-cell activation in vitro, CFDA SE-labeled mouse PBMCs were activated with anti-CD3 and ant-CD28, and treated with UMSC-exos or TAxI-exos (25 μg/well, 1×10^{11} particles mL^{-1}) for 72 h. As shown in **Figure 7a**, T-cell proliferation assays revealed that TAxI-exos and UMSC-exos both suppressed the proliferative capacities of gated T cells. To confirm the effect of UMSC-exos and TAxI-exos on $CD4^+$ and $CD8^+$ T cells, we used FCM **(Fig. 7b, c**). Our results

revealed that TAxI-exos (n = 3, 12.60% ± 0.49%, $p < 0.001$) and UMSC-exos (n = 3, 13.80± 0.23%, $p < 0.001$) significantly decreased the proportion of $CD4^+$ T cells compared with the stimulation group (n = 3, 21.60% ± 0.38%) **(Fig. 7d**). Additionally, TAxI-exos (n = 3, 8.12% ± 0.50%, $p < 0.001$) was more efficient than UMSC-exos (n = 3, 16.63% ± 0.80%, $p < 0.01$) in significantly decreasing the proportion of $CD8^+$ T cells compared with the stimulation group (n = 3, 20.57% ± 0.13%) **(Fig. 7e**).

In vivo, we analyzed the severity of inflammatory cells in treated mouse spinal cord sections by H&E staining (n=3) **(Fig. 7f)**. UMSC-exo- and TAxI-exo-treated groups both showed reductions of inflammatory cells counts in each unit area (1.33 ± 0.58, $p < 0.001$) (1.0± 0, $p < 0.001$) compared with EAE mice ($n = 3$, 3.0± 0) **(Fig. 7g)**.

Recent evidence has confirmed that several pro-inflammatory T cell subsets, particularly Th1 and Th17 cells, are major drivers in MS and EAE [8, 26]. Therefore, we collected cells from spinal cords of UMSC-exo- and TAxI-exo-treated mice. FCM analysis showed that TAxI-exos dramatically reduced percentage of $CD4^+IFN\gamma^+$ T cells (Th1) (n = 3, from 0.74 ± 0.09% to 2.68% ± 0.47% in the EAE group, $p < 0.001$) **(Fig. 7h, i)** and $CD4^+IL\text{-}17^+$ T cells (Th17) (n = 3, from 16.67% ± 2.60% to 29.67% ± 2.85% in the EAE group, $p < 0.01$) **(Fig. 7j, k)**. The effect of UMSC-exos just displayed in Th17 (19.3% ± 1.45%, $p < 0.01$), not Th1.

This study applied in vitro and in vivo models to specifically demonstrate the anti-inflammatory properties of UMSC-exos and TAxI-exos. Both suppressed activation and proliferation of T cells and inhibited the development of Th1 and Th17 cells in EAE mouse spinal cords. Surprisingly, TAxI-exos performed better than UMSC-exos.

UMSC-exos and TAxI-exos induce Tregs to exert immune tolerance in vitro and in vivo

Regulatory T cells (Tregs) are thought to play a critical role in the maintenance of peripheral immune tolerance. Therefore, we assumed that UMSC-exos and TAxI-exos would induce immune tolerance by facilitating the proliferation of Tregs.

To investigate whether UMSC-exos and TAxI-exos induced Tregs in vitro, murine splenocytes from healthy mice were stimulated with anti-CD3 and rIL-2 without some critical factors that drive the generation of Tregs [27] and treated with UMSC-exos, TAxI-exos, or conditioned medium as control. FCM analysis showed that UMSC-exos and TAxI-exos increased the frequency of $CD4^+CD25^+FOXP3^+$ Tregs in vitro: PBS control group (9.96% ± 0.73%, ns), Stimulation group (18.6% ± 0.15%), UMSC-exos group (49.65% ± 4.05%, $p < 0.001$), and TAxI-exos group (68.67% ± 3.45%, $p < 0.001$) ($n = 3$) **(Fig. 8a, b)**. We also determined the percentage of $CD4^+CD25^+FOXP3^+$ Tregs in the spleen in vivo: PBS control group (6.08% ± 0.33%, $p < 0.05$), EAE group (2.69% ± 0.86%), UMSC-exos group (7.84% ± 0.43%, $p < 0.01$), and TAxI-exos group (6.21% ± 0.69%, $p < 0.05$) **(Fig. 8c, d)**. These data showed that UMSC-exos and TAxI-exos promoted the production of Tregs to induce immune tolerance.

UMSC-exos and TAxI-exos reduce expression levels of inflammatory cytokines in vitro and in vivo

To verify the mechanism through which exosomes acted on T cells, cytokines were measured in the T-cell culture medium, serum, and spinal cords of each group.

In culture medium, the levels of IL-2 and IL-17 were significantly reduced by TAxI-exos and UMSC-exos treatments (**Fig. 9a**) and a decreasing trend of IFN-γ was only found in TAxI-exos group (**Fig. 9a**). We were unable to detect other cytokines (data not shown),because their concentrations were below the limit of detection of our assays.

In serum samples, the levels of IL-1β, IL-6, and TNF were decreased notably (**Fig. 9b**), and TGF-β, IL-4, and IL-10 were increased in TAxI-exo-treated mice (**Fig. 9b**). In the presence of UMSC-exos, the trends of most cytokines were not significant, but the level of IL-4 was higher than after TAxI-exo treatment (**Fig. 9b**). Furthermore, we used qRT-PCR to measure expression levels of cytokines in UMSC-exo- or TAxI-exo-treated EAE mouse spinal cords (n=3). The mRNA levels of TNF-α, IL-6, IL-10, and IDO1 were significantly increased after treatments of UMSC-exos and TAxI-exos **(Fig. 9c)**.

These results clearly demonstrated that UMSC-exos and TAxI-exos were capable of immunoregulation by up-regulating the expression levels of anti-inflammatory cytokines, such as IL-4, IL-10, TGF-β, and IDO-1, and down-regulating the expression levels of pro-inflammatory cytokines that IL-1β, IL-2, IL-6, IL-17A, IFN-γ and TNF.

Discussion

Although DMTs development has been continuous for MS in recent years, a limitation of the drugs is that they are only applicable to RRMS [28]. Therefore, we focused on finding a more effective and safer drug. As a classical animal model of MS, EAE was used in this study, which well represents the immune mechanism in MS patients. Because axonal loss is limited to the spinal cord and the minimal demyelination is seen in EAE of C57BL/6 mice [29], which is considered to be a hallmark of MS [30], spinal cord tissues were selected for our analysis. MSCs have been widely reported to possess better clinical curative effects on numerous inflammatory diseases through the paracrine functions of bioactive factors and differentiation into certain functional cells [31, 32]. Previous studies confirmed that UMSC-exos exert an immunoregulatory effect on multiple autoimmune imbalances [33, 34], attenuate tissue injury, and promote tissue repair and regeneration [35]. Meanwhile, UMSC-exos have great BBB-permeability and are suitable for MS therapy [36]. Because of these properties, we chose UMSC-exos for our study. However, when intravenous exosomes are used as a treatment, rapid accumulation occurs in peripheral organs, such as liver and spleen, in EAE [16]. Thus, the targeting characteristic of MSC-exos requires improvement before they can be used for CNS disease therapies. Direct modification of the exosome surface by a CNS-targeting ligand has been shown to enhance CNS tissue retention of exosomes [37]. On the basis of these findings [17, 38], we successfully established TAxI-exos by a post-insertion method using DSPE-PEG2000 [39], that targeted axons of the CNS in EAE models. Furthermore, we determined that systemic injection of TAxI-exos compared with that of UMSC-exos resulted in more

efficient CNS accumulation and BV-2 cells internalization, more sustained clinical recovery with enhanced improvement of motor skills, and more reduction of neuroinflammation and demyelination in EAE mice.

We also investigated the underlying mechanisms. In terms of EAE pathogenesis, we have briefly summarized this with a diagram (Fig. 10). T cells play a major role in inducing and regulating MS pathophysiology, and the development of therapeutics for MS has often focused on targeting factors that mediate T cell functions [40].

Th1 and Th17 cells are the main pathological T cells in the innate immune response of MS and EAE [41]. They produce IFN-γ and IL-17, and infiltrate the brain and spinal cord prior to the development of clinical symptoms in EAE, which activates macrophages/microglia [42]. Thus, the reductions of $CD4^+$ T cells (Th1), $CD8^+$ T cells and Th17 cells may contribute to ameliorating EAE. Our study supported these ideas and demonstrated that TAxI-exos and UMSC-exos inhibited activation and proliferation of T cells and decreased the proportions of $CD4^+$ T and $CD8^+$ T cells in vitro. Additionally, our results suggested that TAxI-exos and UMSC-exos decreased the proportions of Th1 and Th17 cells in the EAE mouse spinal cord and relieved inflammatory cell infiltration of the CNS. Surprisingly, we found that TAxI-exos performed significantly better than UMSC-exos, probably because TAxI peptides provided UMSC-exos with blood stability and targeting ability.

Regulatory T cells (Tregs) are also involved in the pathogenesis of CNS autoimmune inflammation. It is believed that Tregs regulate immune responses in the periphery predominantly by suppressing effector $CD4^+$ T cell subsets that mediate autoimmune responses [43]. Tregs also promote oligodendrocyte differentiation and remyelination [44], which revealed a new regenerative prospect. Studies of MS have shown that a decline expression in $CD25^+$ cells leads to Treg dysfunction during disease progression [45]. Consequently, restoring the Tregs functions prevents development of MS and EAE. In our study, we confirmed that that UMSC-exos and TAxI-exos induced $CD4^+CD25^+FOXP3^+$ Tregs in vitro in the absence of the critical factors. The same result was obtained in vivo. These results suggest that TGFβ and IFN-γ or both from exosomes were provided to the Tregs surface or indirectly other other signals provided on lymphocytes and accessory cells (e.g., B cells, dendritic cells, and antigen-presenting cells), which is in agreement with recent studies showing that Tregs cannot be induced with purified and activated $CD4^+$ T cells [46, 47]. Generally, these data support our hypothesis that UMSC-exos and TAxI-exos ameliorate EAE by suppressing pathological T cell subset activation and induce immune tolerance by promoting Tregs to a certain extent.

Microglia as early immune response cells in gray matter of the spinal cord and brain [48] become activated abnormally, which leads to the demyelination and neurodegeneration in MS and EAE [49]. The next step in microglia activation is an M1/M2 microglia polarization imbalance that is also a major cellular mechanism of MS pathogenesis [50]. M1 microglia cause tissue damage through releasing pro-inflammatory cytokines (TNF-α, IL-6, and iNOS) to accelerate the EAE course [51]. M2 phenotype microglia produce anti-inflammatory cytokines (IL-10 and Arg1) to promote tissue regeneration [12]. When microglial M2 polarization is blocked and halted at the M1 phenotype, the demyelination in EAE

may be exacerbated [52]. Conversely, if polarization of microglia from M1 to M2 is induced, immune homeostasis can be restored and neurological functions improved. Our study focused on the role of TAxI-exos and UMSC-exos in M1/M2 polarization of microglia. The results showed that TAxI-exos enhanced internalization ability of BV-2 cells, reduced the number of $CD86^+CD206^+$ BV-2 cells and $CD86^+$ BV-2 (M1) cells, and elevated the number of $CD206^+$ (M2) cells in vitro. Most likely, the reason for the appearance of $CD86^+CD206^+$ BV-2 cells under LPS stimulation is that BV-2 cells were directed to a transition state between M1 and M2 phenotypes. Additionally, decreasing expression of iNOS and increasing expression of Arg1 were found in spinal cords in vivo. These results also correspond to the expression level of Iba-1 in the spinal cord in which TAxI-exos had a better suppressive effect than UMSC-exos. Taken together, these data indicate that TAxI-exos provide a better delay in the onset of the EAE, which is beneficial to dampen inflammation and promote relief.

Some cytokines are involved in EAE mouse pathology, such as proinflammatory cytokines. For example, IL-1β is secreted from monocytes, IFN-γ and TNFα from Th1 cells, and IL-17A from Th17 cells. Additionally, anti-inflammatory cytokines are involved, such as IL-4, IL-6, and IL-10 from Th2 cells, and TGF-β that is important for Tregs proliferation. IL-6 and IL-1β are also important activators of Th17 cells that differentiate from native CD4+ T cells [9]. A major function of IL-17A in autoimmunity of CNS is to recruit IL-1β-secreting myeloid cells that prime pathological γδT17 and Th17 cells [53]. IL-6 is also a Th2 cell-secreted cytokine that is positively correlated with the numbers of Th2 cells that inhibit Th1 cell proliferation and participate in humoral immunity by secreting anti-inflammatory cytokines such as IL-10 [54]. IDO1 is an immunosuppressive enzyme screened from exosomes with good immunosuppressive effects on T cell proliferation [55, 56]. Our study analyzed the levels of these cytokines in vitro and in vivo. The data demonstrated that treatment with TAxI-exos or UMSC-exos increased the mRNA levels of IL-6, IL10, IDO-1, and TNF-α in the spinal cord; reduced the concentrations of IL-1β, IL-6, and TNF-α, and increased the concentration of IL-4, IL-10, and TGF-β in the serum of EAE mice; and reduced the concentrations of IL-2, IL-17A, and IFN-γ in culture medium. These data helped to reveal the anti-inflammatory mechanisms of exosomes. We found that the levels of IL-4 and IL-10 were commonly increased in periphery and in spinal cord after TAxI-exo-treatment. It indicated that the anti-inflammatory effect of TAxI-exos was partially mediated by boosting the production of cytokines from Th2 or Th2 cells themselves. Additionally, the declining levels of IL-2, IFN-γ, and IL-17A in culture medium indicated that Th1 and Th17 cells were effectively inhibited by TAxI-exos or UMSC-exos, which contributed to immunosuppression of EAE. By the way, the expression level of TNF was down-regulated in serum, but up-regulated in spinal cord. One possible reason is that TNF was ablated in monocytes/macrophages but not in microglia, which delayed the onset of EAE and was associated with reduced acute spinal cord infiltration of monocytes [57]. Ultimately, the therapeutic effects of TAxI-exos or UMSC-exos were achieved partially by regulating the levels of inflammatory cytokines in our study.

Because of their small size and enrichment steps, compared with the MSCs, exosome-based therapeutics have many advantages in terms of safety and convenience, and can be considered as a surrogate treatment to cell therapy. Our results suggest that TAxI-exos perform better than native exosomes (UMSC-

exos) in many aspects because of their central nervous system-targeting ability. A study has shown that TAxI peptides have no adverse effects on mice [17]. The successful establishment and application of TAxI-exos in the mouse EAE model may contribute to treating other immune diseases such as MS. They can also be used as a targeted drug delivery vehicle for CNS diseases in the future.

Although our results suggest that TAxI-exos have a good therapeutic effect on EAE in mice, this study has some limitations. Despite the axon-targeting ability of TAxI, the specific target cells in axons are not yet clear. We only chose microglia as the candidate in our study. More precise target cells of the TAxI peptide need to be explored further. The pathogenesis of MS involves many immune cells, and we just focused on $CD4^+$ T cells, $CD8^+$ T cells, Th17 cells, and Tregs both in vivo and in vitro. Therefore, it is necessary to explore the mechanisms with of immune cells in EAE. Additionally, the therapeutic effect of TAxI-exos in other suitable animal models, such as spinal cord injury, should be assessed in future studies.

Conclusion

Our study is the first to develop a CNS-targeting cell-free therapy for MS and EAE using TAxI peptides and UMSC-exos, named TAxI-exos. TAxI-exos enhanced the therapeutic effect of UMSC-exos by improving the CNS-targeting ability. Our work also helped to understand the mechanism of immune regulation, immunosuppression, and induction of immune tolerance of UMSC-exos in EAE. TAxI-exos have great promise for other autoimmune and neurodegenerative diseases in the future.

Abbreviations

MS, multiple sclerosis; EAE, Experimental autoimmune encephalomyelitis; CNS, Central nervous system; DMTs, disease-modifying therapies; RRMS, relapsing remitting multiple sclerosis; SPMS, secondary progressive multiple sclerosis; BBB, blood-brain barrier; Th1, helper T cell 1; Th17, helper T cell 17; Tregs, regulatory T cells; MSCs, mesenchymal stem cells; UC-MSCs, human umbilical cord tissue-derived MSCs; UMSC-exos, umbilical cord MSCs exosomes; TAxI-exos, TAxI-modified UMSC-exos; FBS, fetal bovine serum; RT, room temperature; PBS, Phosphate-buffered saline; TEM, transmission electron microscope; NTA, nanoparticle tracking analysis; DiR,1,1'-dioctadecyl-3,3,3',3-tetramethylindocarbocyanine iodide; CFDA SE, 5,6-carboxyfluorescein diacetate, succinimidyl ester; LFB, Luxol fast blue; WB, western blot; FCM, Flow cytometry; PBMCs, peripheral blood mononuclear lymphocytes; CBA, cytometric bead array; MFI, mean fluorescence intensity; qRT-PCR, quantitative reverse transcription-PCR; MBP, myelin basic protein; LPS, lipopolysaccharide.

Declarations

Ethic approval and consent to participate

All animals and experiments in this study were approved by the Animal Ethics Committee of Xiamen Medical College (Approval ID: 20190302007).

All human umbilical cords in this study were approved by Medical Ethics Committee of Zhongshan Hospital affiliated to Xiamen University (Approval ID: xmzsyyky (2021-106))

Consent for publication

Not applicable

Availability of data and materials

All data used in this study are available from the correspongding author on reasonable request.

Competing interests

The authors declare that they have no competing interests.

Funding

This study was supported by grants from the National Key Technology R&D Program of China (2018YFA0108304), the National Natural Science Foundation of China (81771721, 81971505, 81901631), and key laboratory of functional and clinical translational medicine, Fujian province university (XMMC-FCTM201905)

Author's contributions

Z.Q. Qi made contributions to experimental design manuscript revision and funding. Y.K. Wang performed the experiments, analyzed the data, and drafted the article. M.Z. Ye, Y. Wang, Y.P Zhao, L. Wang provided experimental materials. T.S. Lan made contribution to the funding.

Acknowledgements

The authors thank Wang-Xiao He, College of Life Sciences and Technology, Xi'an Jiaotong University, for his help in designing of TAxI modification strategy. We also thank Hua-Xiu Sui, Key laboratory of functional and clinical translational medicine, Fujian province university, Xiamen Medical College, for her technical assistance.

Authors' information

Y.K. W, MD

School of Medicine, Guangxi University, Nanning, Guangxi, China.

E-mail: 1143908521@qq.com

Y.P. Z, PhD

Research Center of Developmental Biology, Department of Histology and Embryology College of Basic Medicine, Naval Medical University, Shanghai, China.

E-mail: jane124600@163.com

M.Z. Y, PhD

Department of Obstetrics and Gynecology, Zhong Shan Hospital, Xiamen University Xiamen Fujian China.

E-mail: mingzhu875702@163.com

L. W, MD

Translational medicine research center, the navy medical university, Shanghai, China

E-mail:wl201506@126.com

References

1. Howard J, Trevick S, Younger DS: **Epidemiology of Multiple Sclerosis**. *Neurol Clin* 2016, **34**(4):919–939.
2. Correale J, Gaitan MI, Ysrraelit MC, Fiol MP: **Progressive multiple sclerosis: from pathogenic mechanisms to treatment**. *Brain* 2017, **140**(3):527–546.
3. Jalkh G, Abi Nahed R, Macaron G, Rensel M: **Safety of Newer Disease Modifying Therapies in Multiple Sclerosis**. *Vaccines (Basel)* 2020, **9**(1).
4. An K, Xue MJ, Zhong JY, Yu SN, Lan TS, Qi ZQ, Xia JJ: **Arsenic trioxide ameliorates experimental autoimmune encephalomyelitis in C57BL/6 mice by inducing CD4(+) T cell apoptosis**. *J Neuroinflammation* 2020, **17**(1):147.
5. Filippini G, Del Giovane C, Clerico M, Beiki O, Mattoscio M, Piazza F, Fredrikson S, Tramacere I, Scalfari A, Salanti G: **Treatment with disease-modifying drugs for people with a first clinical attack suggestive of multiple sclerosis**. *Cochrane Database Syst Rev* 2017, **4**:CD012200.
6. Glatigny S, Bettelli E: **Experimental Autoimmune Encephalomyelitis (EAE) as Animal Models of Multiple Sclerosis (MS)**. *Cold Spring Harb Perspect Med* 2018, **8**(11).
7. Rangachari M, Kuchroo VK: **Using EAE to better understand principles of immune function and autoimmune pathology**. *J Autoimmun* 2013, **45**:31–39.
8. Kaskow BJ, Baecher-Allan C: **Effector T Cells in Multiple Sclerosis**. *Cold Spring Harb Perspect Med* 2018, **8**(4).

9. McGinley AM, Edwards SC, Raverdeau M, Mills KHG: **Th17cells, gammadelta T cells and their interplay in EAE and multiple sclerosis**. *J Autoimmun* 2018.
10. Kamali AN, Noorbakhsh SM, Hamedifar H, Jadidi-Niaragh F, Yazdani R, Bautista JM, Azizi G: **A role for Th1-like Th17 cells in the pathogenesis of inflammatory and autoimmune disorders**. *Mol Immunol* 2019, **105**:107–115.
11. Van Kaer L, Postoak JL, Wang C, Yang G, Wu L: **Innate, innate-like and adaptive lymphocytes in the pathogenesis of MS and EAE**. *Cell Mol Immunol* 2019, **16**(6):531–539.
12. Li Z, Liu F, He X, Yang X, Shan F, Feng J: **Exosomes derived from mesenchymal stem cells attenuate inflammation and demyelination of the central nervous system in EAE rats by regulating the polarization of microglia**. *Int Immunopharmacol* 2019, **67**:268–280.
13. Ceccariglia S, Cargnoni A, Silini AR, Parolini O: **Autophagy: a potential key contributor to the therapeutic action of mesenchymal stem cells**. *Autophagy* 2020, **16**(1):28–37.
14. Luz-Crawford P, Kurte M, Bravo-Alegria J, Contreras R, Nova-Lamperti E, Tejedor G, Noel D, Jorgensen C, Figueroa F, Djouad F *et al*: **Mesenchymal stem cells generate a CD4+CD25+Foxp3+ regulatory T cell population during the differentiation process of Th1 and Th17 cells**. *Stem Cell Res Ther* 2013, **4**(3):65.
15. Toh WS, Lai RC, Zhang B, Lim SK: **MSC exosome works through a protein-based mechanism of action**. *Biochem Soc Trans* 2018, **46**(4):843–853.
16. Riazifar M, Mohammadi MR, Pone EJ, Yeri A, Lasser C, Segaliny AI, McIntyre LL, Shelke GV, Hutchins E, Hamamoto A *et al*: **Stem Cell-Derived Exosomes as Nanotherapeutics for Autoimmune and Neurodegenerative Disorders**. *ACS Nano* 2019, **13**(6):6670–6688.
17. Sellers DL, Tan JY, Pineda JMB, Peeler DJ, Porubsky VL, Olden BR, Salipante SJ, Pun SH: **Targeting Ligands Deliver Model Drug Cargo into the Central Nervous System along Autonomic Neurons**. *ACS Nano* 2019, **13**(10):10961–10971.
18. Gramlich OW, Brown AJ, Godwin CR, Chimenti MS, Boland LK, Ankrum JA, Kardon RH: **Systemic Mesenchymal Stem Cell Treatment Mitigates Structural and Functional Retinal Ganglion Cell Degeneration in a Mouse Model of Multiple Sclerosis**. *Transl Vis Sci Technol* 2020, **9**(8):16.
19. Seshareddy K, Troyer D, Weiss ML: **Method to isolate mesenchymal-like cells from Wharton's Jelly of umbilical cord**. *Methods Cell Biol* 2008, **86**:101–119.
20. Uder C, Bruckner S, Winkler S, Tautenhahn HM, Christ B: **Mammalian MSC from selected species: Features and applications**. *Cytometry A* 2018, **93**(1):32–49.
21. Kooijmans SAA, Fliervoet LAL, van der Meel R, Fens M, Heijnen HFG, van Bergen En Henegouwen PMP, Vader P, Schiffelers RM: **PEGylated and targeted extracellular vesicles display enhanced cell specificity and circulation time**. *J Control Release* 2016, **224**:77–85.
22. Jung MK, Mun JY: **Sample Preparation and Imaging of Exosomes by Transmission Electron Microscopy**. *J Vis Exp* 2018(131).
23. Goschl L, Scheinecker C, Bonelli M: **Treg cells in autoimmunity: from identification to Treg-based therapies**. *Semin Immunopathol* 2019, **41**(3):301–314.

24. Dominici M, Le Blanc K, Mueller I, Slaper-Cortenbach I, Marini F, Krause D, Deans R, Keating A, Prockop D, Horwitz E: **Minimal criteria for defining multipotent mesenchymal stromal cells. The International Society for Cellular Therapy position statement**. *Cytotherapy* 2006, **8**(4):315–317.
25. Nikfarjam S, Rezaie J, Zolbanin NM, Jafari R: **Mesenchymal stem cell derived-exosomes: a modern approach in translational medicine**. *J Transl Med* 2020, **18**(1):449.
26. McWilliams IL, Rajbhandari R, Nozell S, Benveniste E, Harrington LE: **STAT4 controls GM-CSF production by both Th1 and Th17 cells during EAE**. *J Neuroinflammation* 2015, **12**:128.
27. Liu M, Li S, Li MO: **TGF-beta Control of Adaptive Immune Tolerance: A Break From Treg Cells**. *Bioessays* 2018, **40**(11):e1800063.
28. Hauser SL, Cree BAC: **Treatment of Multiple Sclerosis: A Review**. *Am J Med* 2020, **133**(12):1380-1390 e1382.
29. Burrows DJ, McGown A, Jain SA, De Felice M, Ramesh TM, Sharrack B, Majid A: **Animal models of multiple sclerosis: From rodents to zebrafish**. *Mult Scler* 2019, **25**(3):306–324.
30. Thompson AJ, Baranzini SE, Geurts J, Hemmer B, Ciccarelli O: **Multiple sclerosis**. *The Lancet* 2018, **391**(10130):1622–1636.
31. Dong R, Liu Y, Yang Y, Wang H, Xu Y, Zhang Z: **MSC-Derived Exosomes-Based Therapy for Peripheral Nerve Injury: A Novel Therapeutic Strategy**. *Biomed Res Int* 2019, **2019**:6458237.
32. Regmi S, Pathak S, Kim JO, Yong CS, Jeong JH: **Mesenchymal stem cell therapy for the treatment of inflammatory diseases: Challenges, opportunities, and future perspectives**. *Eur J Cell Biol* 2019, **98**(5-8):151041.
33. Zhao J, Chen J, Huang F, Wang J, Su W, Zhou J, Qi Q, Cao F, Sun B, Liu Z *et al*: **Human gingiva tissue-derived MSC ameliorates immune-mediated bone marrow failure of aplastic anemia via suppression of Th1 and Th17 cells and enhancement of CD4+Foxp3+ regulatory T cells differentiation**. *Am J Transl Res* 2019, **11**(12):7627–7643.
34. Farinazzo A, Angiari S, Turano E, Bistaffa E, Dusi S, Ruggieri S, Bonafede R, Mariotti R, Constantin G, Bonetti B: **Nanovesicles from adipose-derived mesenchymal stem cells inhibit T lymphocyte trafficking and ameliorate chronic experimental autoimmune encephalomyelitis**. *Sci Rep* 2018, **8**(1):7473.
35. Thomi G, Joerger-Messerli M, Haesler V, Muri L, Surbek D, Schoeberlein A: **Intranasally Administered Exosomes from Umbilical Cord Stem Cells Have Preventive Neuroprotective Effects and Contribute to Functional Recovery after Perinatal Brain Injury**. *Cells* 2019, **8**(8).
36. Otero-Ortega L, Laso-Garcia F, Gomez-de Frutos M, Fuentes B, Diekhorst L, Diez-Tejedor E, Gutierrez-Fernandez M: **Role of Exosomes as a Treatment and Potential Biomarker for Stroke**. *Transl Stroke Res* 2019, **10**(3):241–249.
37. Chung EP, Cotter JD, Prakapenka AV, Cook RL, DiPerna DM, Sirianni RW: **Targeting Small Molecule Delivery to the Brain and Spinal Cord via Intranasal Administration of Rabies Virus Glycoprotein (RVG29)-Modified PLGA Nanoparticles**. *Pharmaceutics* 2020, **12**(2).

38. Sellers DL, Bergen JM, Johnson RN, Back H, Ravits JM, Horner PJ, Pun SH: **Targeted axonal import (TAxI) peptide delivers functional proteins into spinal cord motor neurons after peripheral administration**. *Proc Natl Acad Sci U S A* 2016, **113**(9):2514–2519.
39. Zhu Q, Ling X, Yang Y, Zhang J, Li Q, Niu X, Hu G, Chen B, Li H, Wang Y *et al*: **Embryonic Stem Cells-Derived Exosomes Endowed with Targeting Properties as Chemotherapeutics Delivery Vehicles for Glioblastoma Therapy**. *Adv Sci (Weinh)* 2019, **6**(6):1801899.
40. Baecher-Allan C, Kaskow BJ, Weiner HL: **Multiple Sclerosis: Mechanisms and Immunotherapy**. *Neuron* 2018, **97**(4):742–768.
41. Fletcher JM, Lalor SJ, Sweeney CM, Tubridy N, Mills KH: **T cells in multiple sclerosis and experimental autoimmune encephalomyelitis**. *Clin Exp Immunol* 2010, **162**(1):1–11.
42. Murphy AC, Lalor SJ, Lynch MA, Mills KH: **Infiltration of Th1 and Th17 cells and activation of microglia in the CNS during the course of experimental autoimmune encephalomyelitis**. *Brain Behav Immun* 2010, **24**(4):641–651.
43. Danikowski KM, Jayaraman S, Prabhakar BS: **Regulatory T cells in multiple sclerosis and myasthenia gravis**. *J Neuroinflammation* 2017, **14**(1):117.
44. Dombrowski Y, O'Hagan T, Dittmer M, Penalva R, Mayoral SR, Bankhead P, Fleville S, Eleftheriadis G, Zhao C, Naughton M *et al*: **Regulatory T cells promote myelin regeneration in the central nervous system**. *Nat Neurosci* 2017, **20**(5):674–680.
45. Mexhitaj I, Nyirenda MH, Li R, O'Mahony J, Rezk A, Rozenberg A, Moore CS, Johnson T, Sadovnick D, Collins DL *et al*: **Abnormal effector and regulatory T cell subsets in paediatric-onset multiple sclerosis**. *Brain* 2019, **142**(3):617–632.
46. Zhang B, Yeo RWY, Lai RC, Sim EWK, Chin KC, Lim SK: **Mesenchymal stromal cell exosome-enhanced regulatory T-cell production through an antigen-presenting cell-mediated pathway**. *Cytotherapy* 2018, **20**(5):687–696.
47. Zhang Q, Fu L, Liang Y, Guo Z, Wang L, Ma C, Wang H: **Exosomes originating from MSCs stimulated with TGF-beta and IFN-gamma promote Treg differentiation**. *J Cell Physiol* 2018, **233**(9):6832–6840.
48. Madore C, Yin Z, Leibowitz J, Butovsky O: **Microglia, Lifestyle Stress, and Neurodegeneration**. *Immunity* 2020, **52**(2):222–240.
49. Chu F, Shi M, Zheng C, Shen D, Zhu J, Zheng X, Cui L: **The roles of macrophages and microglia in multiple sclerosis and experimental autoimmune encephalomyelitis**. *J Neuroimmunol* 2018, **318**:1–7.
50. Mazzon C, Zanotti L, Wang L, Del Prete A, Fontana E, Salvi V, Poliani PL, Sozzani S: **CCRL2 regulates M1/M2 polarization during EAE recovery phase**. *J Leukoc Biol* 2016, **99**(6):1027–1033.
51. Kwon HS, Koh SH: **Neuroinflammation in neurodegenerative disorders: the roles of microglia and astrocytes**. *Transl Neurodegener* 2020, **9**(1):42.
52. Sun D, Yu Z, Fang X, Liu M, Pu Y, Shao Q, Wang D, Zhao X, Huang A, Xiang Z *et al*: **LncRNA GAS5 inhibits microglial M2 polarization and exacerbates demyelination**. *EMBO Rep* 2017, **18**(10):1801–1816.

53. McGinley AM, Sutton CE, Edwards SC, Leane CM, DeCourcey J, Teijeiro A, Hamilton JA, Boon L, Djouder N, Mills KHG: **Interleukin-17A Serves a Priming Role in Autoimmunity by Recruiting IL-1beta-Producing Myeloid Cells that Promote Pathogenic T Cells**. *Immunity* 2020, **52**(2):342-356 e346.
54. Metaxakis A, Petratou D, Tavernarakis N: **Molecular Interventions towards Multiple Sclerosis Treatment**. *Brain Sci* 2020, **10**(5).
55. Mondanelli G, Coletti A, Greco FA, Pallotta MT, Orabona C, Iacono A, Belladonna ML, Albini E, Panfili E, Fallarino F *et al*: **Positive allosteric modulation of indoleamine 2,3-dioxygenase 1 restrains neuroinflammation**. *Proc Natl Acad Sci U S A* 2020, **117**(7):3848-3857.
56. Merlo LMF, DuHadaway JB, Montgomery JD, Peng WD, Murray PJ, Prendergast GC, Caton AJ, Muller AJ, Mandik-Nayak L: **Differential Roles of IDO1 and IDO2 in T and B Cell Inflammatory Immune Responses**. *Front Immunol* 2020, **11**:1861.
57. Wolf Y, Shemer A, Polonsky M, Gross M, Mildner A, Yona S, David E, Kim KW, Goldmann T, Amit I *et al*: **Autonomous TNF is critical for in vivo monocyte survival in steady state and inflammation**. *J Exp Med* 2017, **214**(4):905–917.

Figures

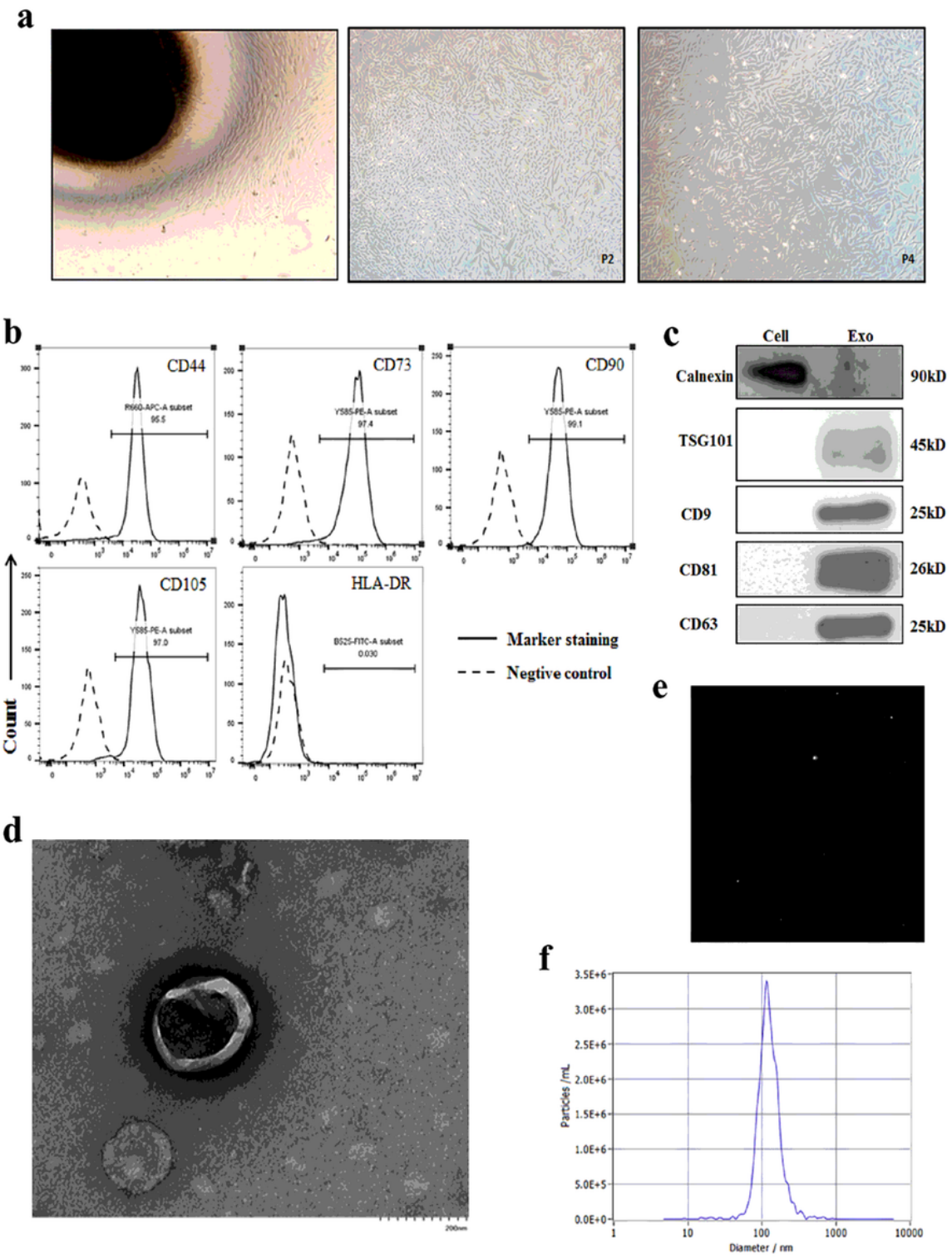

Figure 1

Characterization of UMSCs and UMSC-exos. (a) Representative micrographs of human umbilical cord mesenchymal stem cells, ×400.(b) hUMSCs surface antigenic features of HLA-DR、CD44、CD90、CD105 and CD73 were analyzed by flow cytometry. (c) The protein levels of Calnexin, CD9, TSG101,CD81 in hUMSCs exosomes and the parental cells were analyzed by western blot.(d) Representative TEM image

of exosomes derived from hUMSCs. Scale bar, 200 nm. The exosomes were analyzed by NTA, (e) a screenshot of the NTA video, (f) the average diameter is 116.6 ± 3nm.

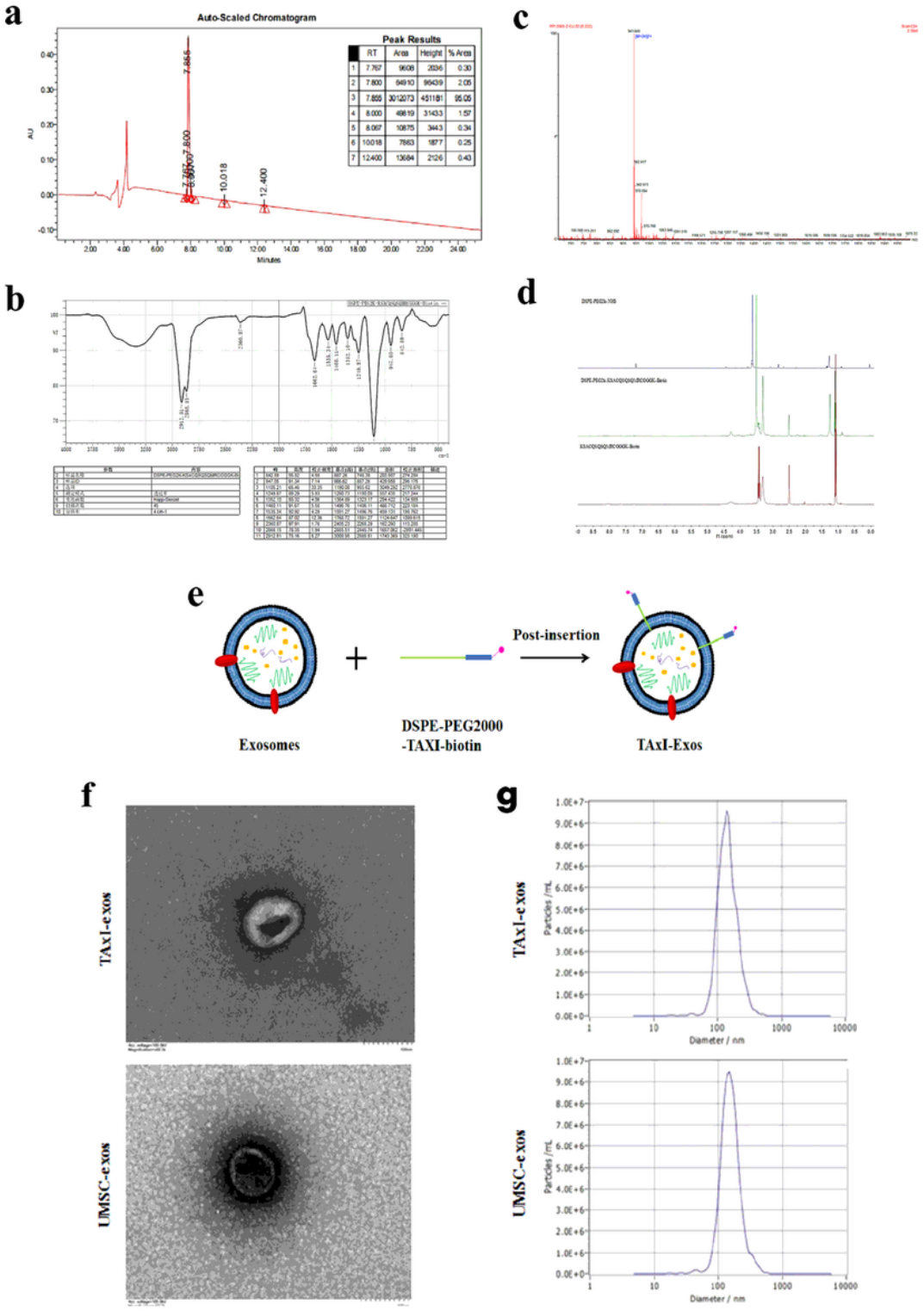

Figure 2

CNS-targeting modification of UMSC-exos and identification of TAxI peptides, DSPE-PEG2000-TAxI, and TAxI-exos. (a, b) TAxI peptides were analyzed using HPLC and MS, the purity was 95.05% and molecular weight was 1880.2. (c, d) DSPE-PEG2000-TAxI were identified by IR and NMR. (e) Schematic diagram of

conjugating TAxI peptides with UMSC-exos. (f) Representative transmission electron micrographs of UMSC-exos and TAxI-exos. Scale bar, 200 nm. (g) The particle size distribution of UMSC-exos and TAxI-exos analyzed by NTA. The average diameter of UMSC-exos is 138.4 nm, and TAxI-Exo is 150.6 nm.

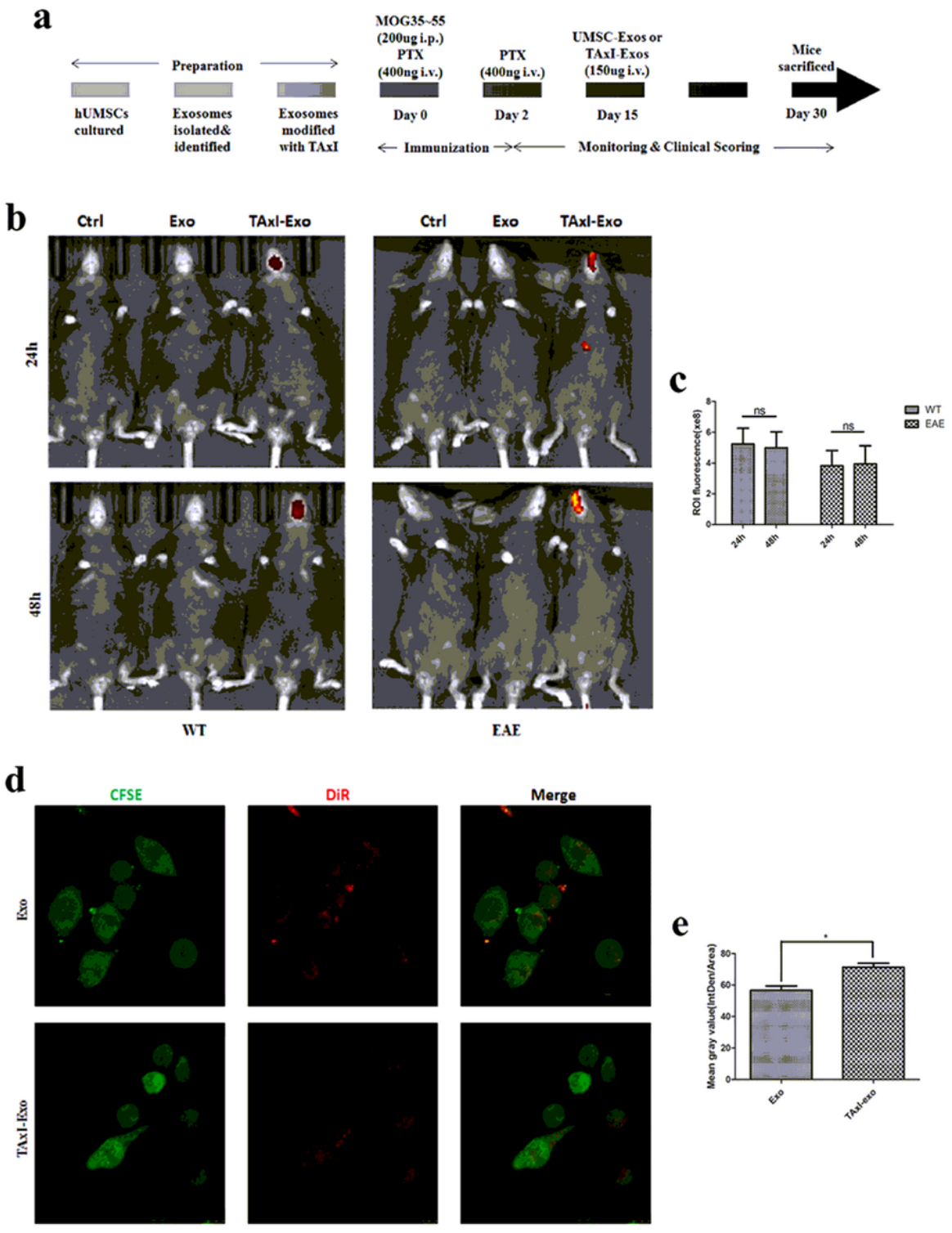

Figure 3

Targeting capability of TAxI-exos in vivo and in vitro. (a) Schematic representation of the procedure to induce EAE and the treatment of UMSC-exos or TAxI-exos. (b) The fluorescence images of UMSC-exos or

the TAxI-exos in vivo at 24 and 48 h after intravenous injection, (c) and quantification of fluorescence intensity by the Spectrum/CT software (n = 3). (d) Representative fluorescence images of the internalization of DiR-labeled UMSC-exos or TAxI-exos in CFSE-labeled BV-2 cells after 12 h. Scale bar, 25 μm. (e) The quantification of fluorescence intensity by the Spectrum/CT software (n = 3) . *p < 0.05, **p < 0.01, ***p < 0.01, ns: no significantly difference.

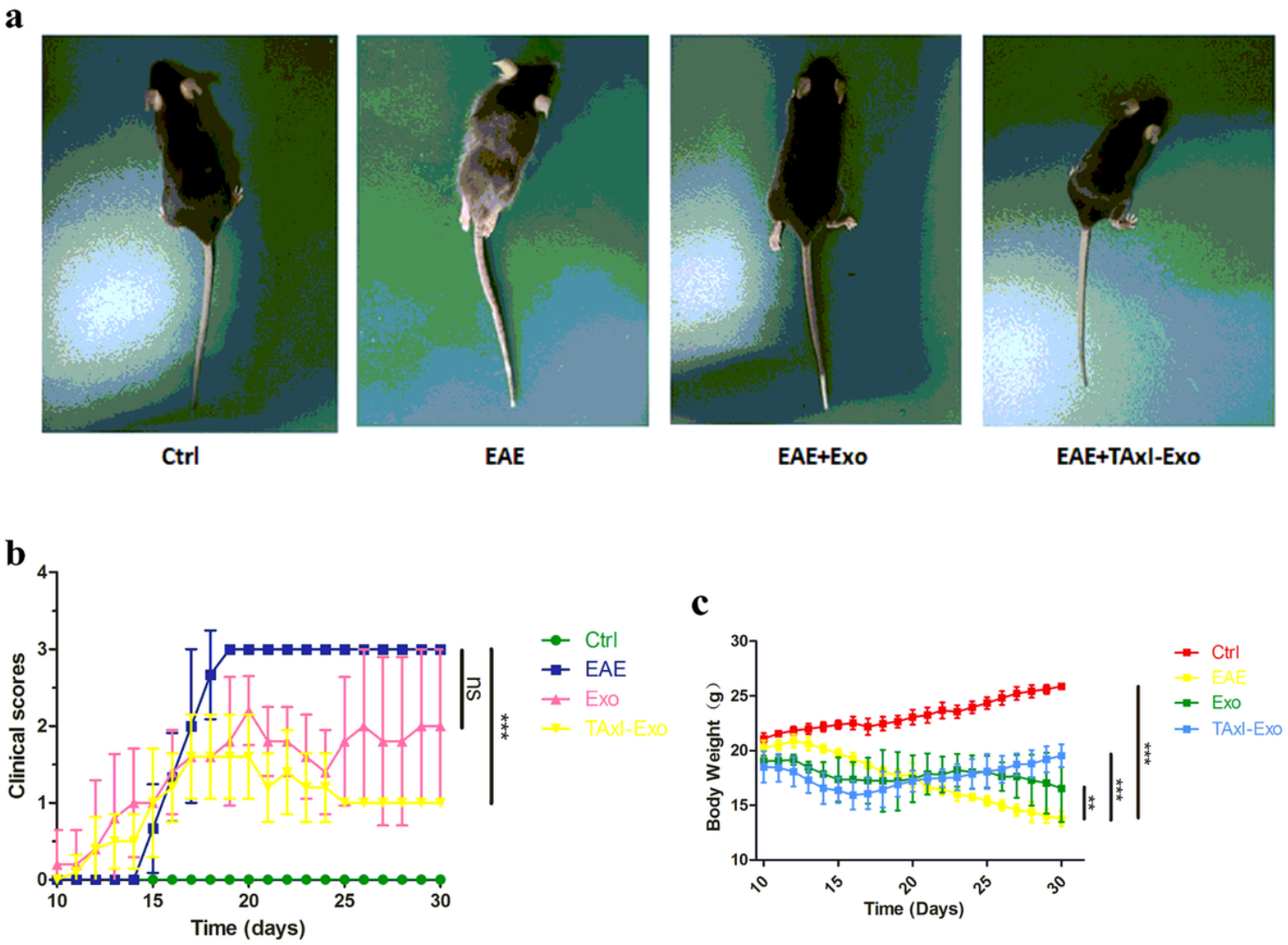

Figure 4

UMSC-exos and TAxI-exos ameliorate EAE progression in mice. (a) Representative images show behavioral symptoms of EAE mice in individual experimental groups, especially hind limb paralysis. (b)The clinical scores and (c) changes in body weight were recorded (n = 5). *p < 0.05, **p < 0.01, ***p < 0.001, ns: no significantly difference.

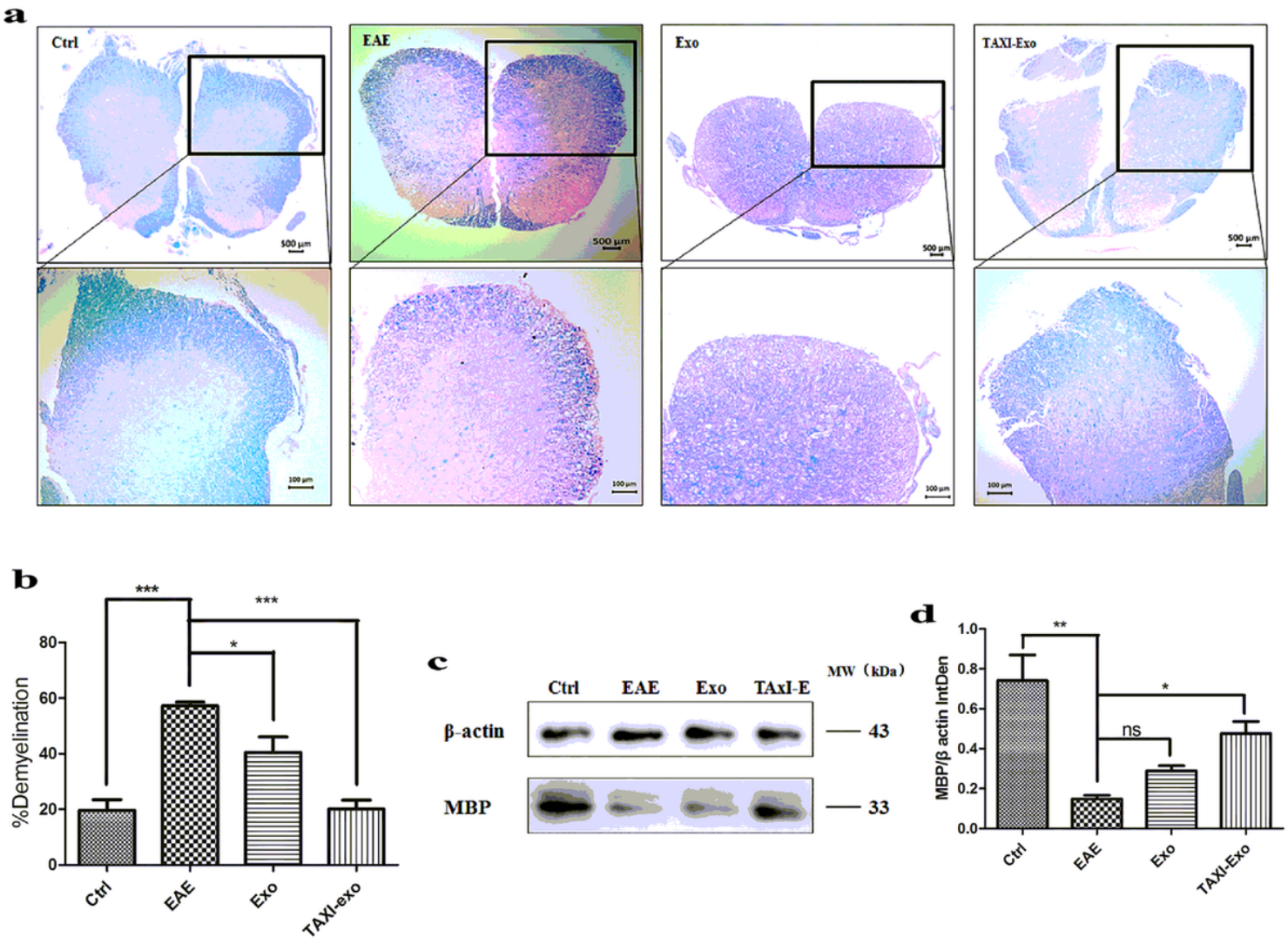

Figure 5

UMSC-exos and TAxI-exos alleviate demyelination in the spinal cord of EAE mice. (a)Representative LFB staining sections images at ×50 microscope with scale bar 500 μm and ×100 microscope with scale bar 100 μm. (b) Percentage of demyelination area of LFB spinal cord (n = 3). (c) Western blotting of MBP protein level in spinal cord (n = 3), (d) and quantification of the gray value. *p < 0.05, **p < 0.01, ***p < 0.001, ns: no significantly difference.

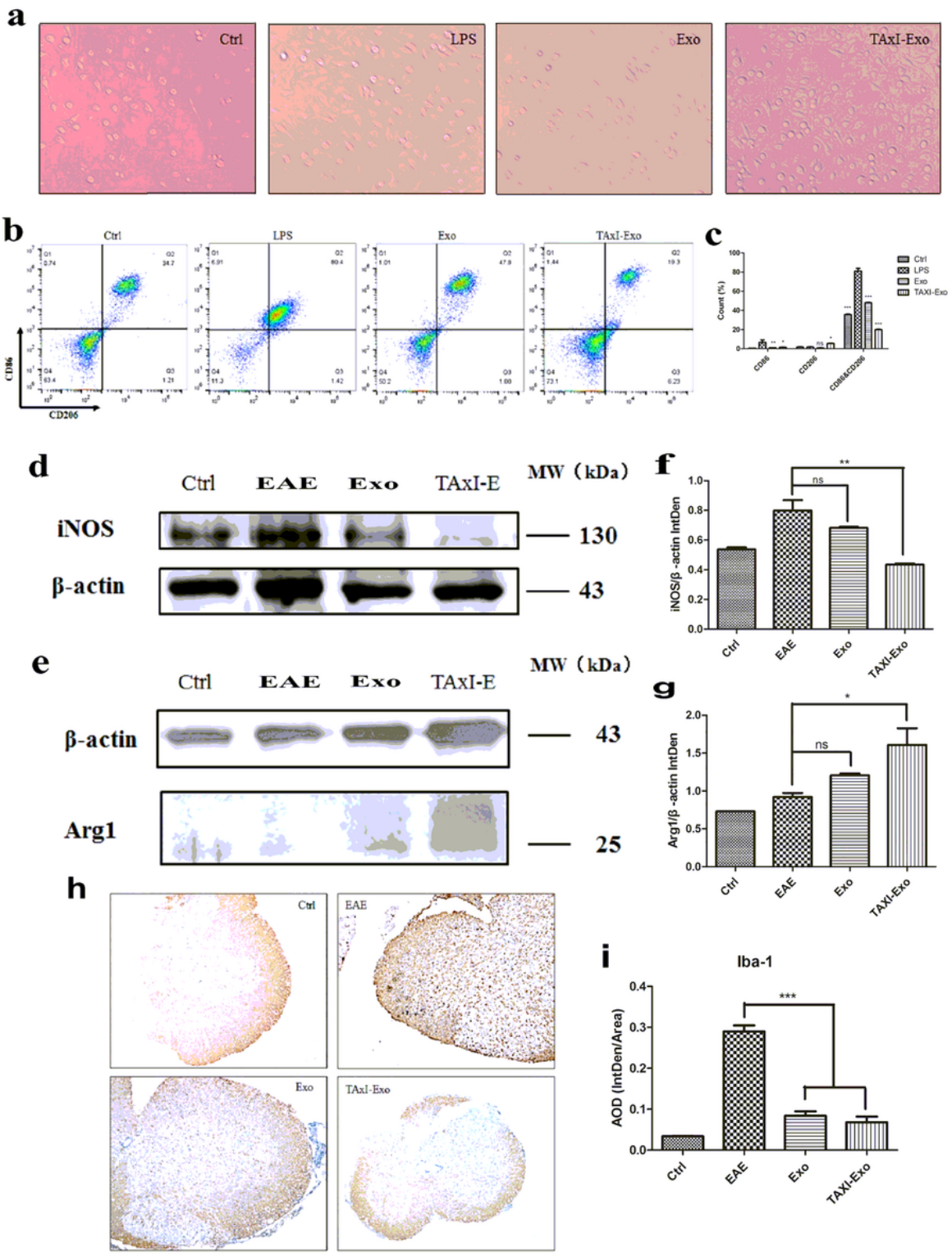

Figure 6

UMSC-exos and TAxI-exos inhibit M1 phenotype polarization and promotes M2 polarization of microglia in vitro and reduce the proportion of macrophage/microglia in vivo. (a) Representative micrographs of BV-2 cells with different treatment, ×400. (b) Representative flow cytometry plots of M1 phenotype marker (CD86) and M2 phenotype marker (CD206) on BV2 cells surfaces (c) and its quantification. (d, e) Representative western blotting of M1 phenotype marker (iNOS) and M2 phenotype marker (Arg1) in mice

spinal cords, (f, g) the levels of proteins were quantified. (H) Immunohistochemical staining of Iba-1 was performed in spinal cord. ×100, scale bar 100μm. (I) Analysis of the infiltration of Iba-1 in spinal cord using average optical density (AOD) (n = 3). *p < 0.05, **p < 0.01, ***p < 0.001, ns: no significantly difference.

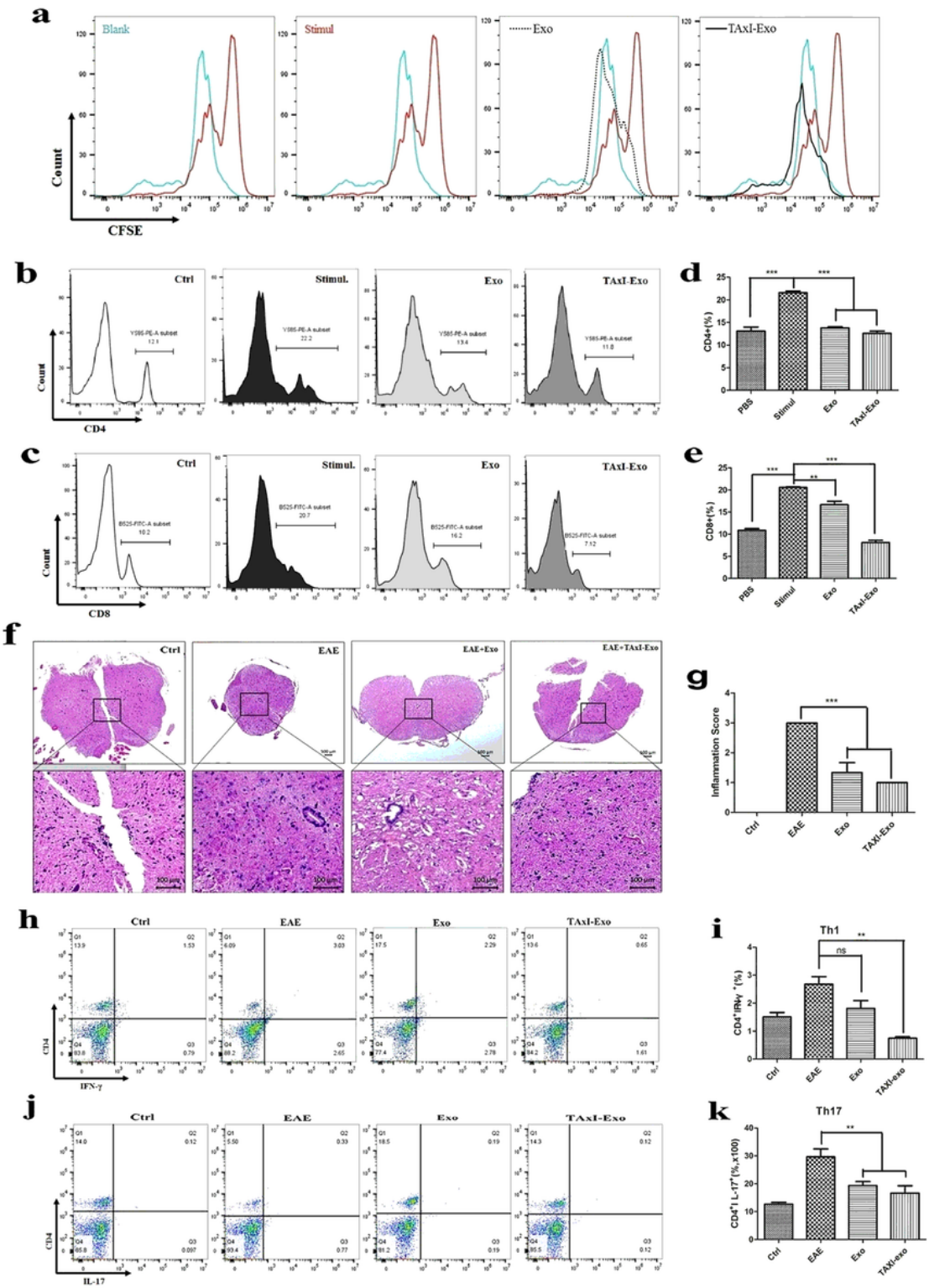

Figure 7

UMSC-exos and TAxI-exos have immunosuppressive effects on T cells in vitro and in vivo. (a) Healthy mice PBMCs were labeled with CFSE and activated for 3 d with antiCD3&CD28, at same time incubated with UMSC-exos or TAxI-exos. (b, c)Addition of UMSC-exos or TAxI-exos to the PBMCs culture decreased the proportions of CD4+ and CD8+ T cells. (d, e) The quantification of flow cytometry plots. (f) H&E staining show that UMSC-exos and TAxI-exos attenuated the infiltration of inflammatory cells in mice spinal cords. ×50, 500 μm or ×100, 100 μm. (g) Inflammation scores was quantified. Representative flow cytometry plots of (h) CD4+IFN-γ+ T cells (Th1) and (j) CD4+IL-17+ T cells (Th17), (i, k) those proportion were quantified.*$p < 0.05$, **$p < 0.01$, ***$p < 0.001$, ns: no significantly difference.

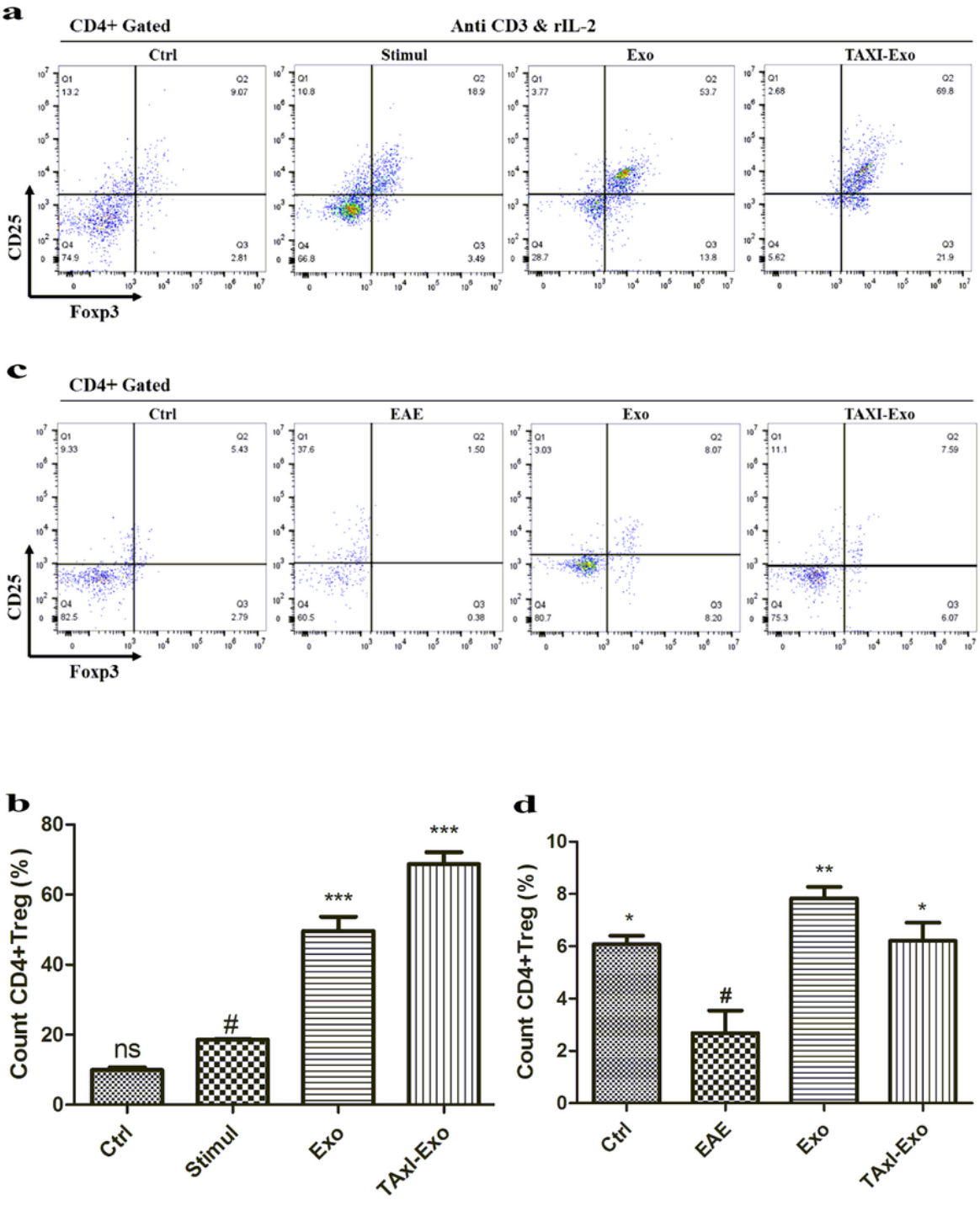

Figure 8

UMSC-exos and TAxI-exos promote Tregs proliferation to induce immune tolerance in vitro and in vivo. Healthy mice splenocytes were stimulated with anti-CD3&rIL-2, and were further cultured 3 day with indicated concentrations of UMSC-exos or TAxI-exos. (a) Representative FACS plots of CD4+ gate (b) and its quantification. (c, d) The splenocytes from each experimental groups were collected, and the

proportion of CD25+&Foxp3+ on CD4+ gate was analyzed by FCM. *p < 0.05, **p < 0.01, ***p < 0.001, ns: no significantly difference.

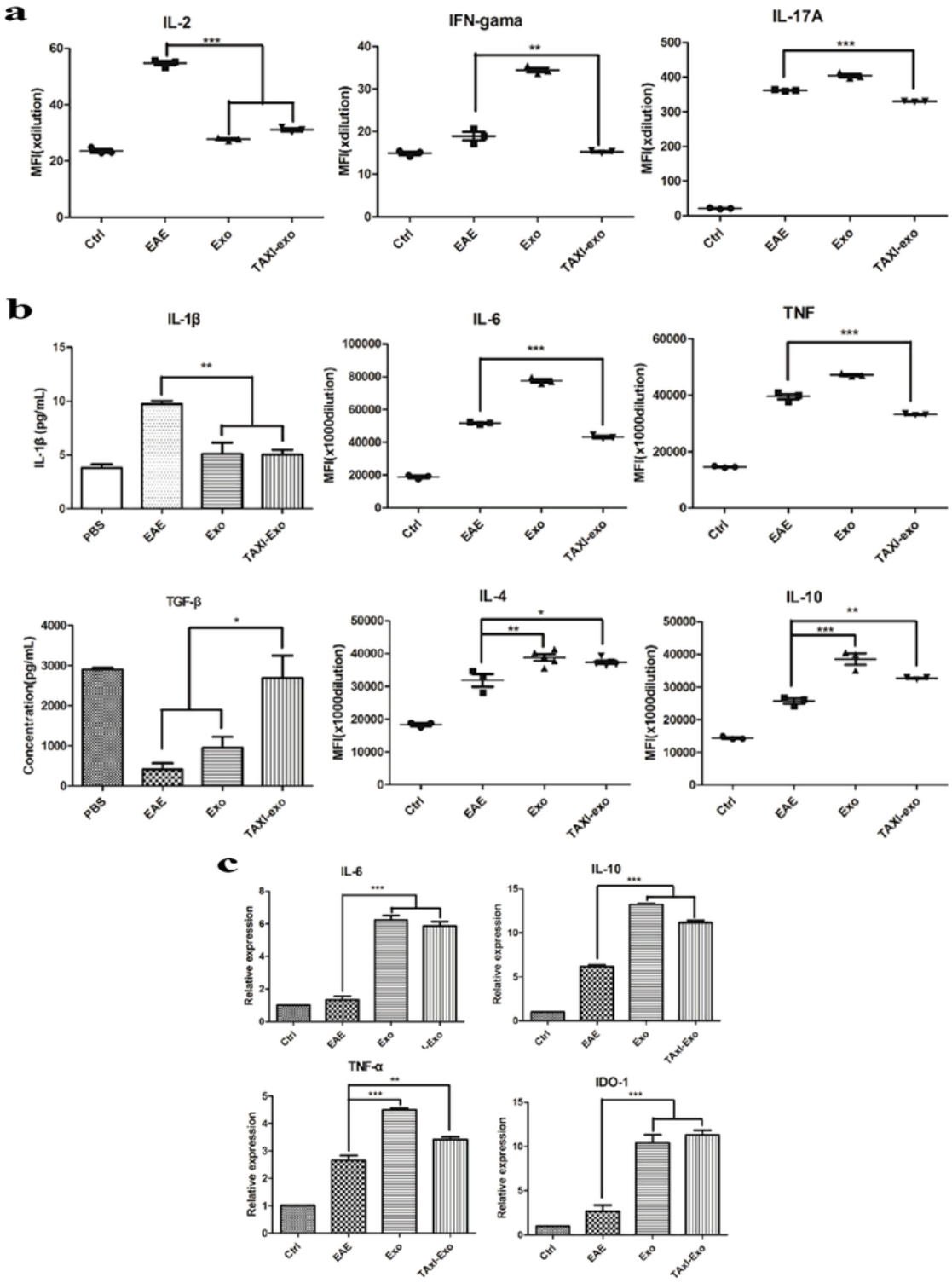

Figure 9

UMSC-exos and TAxI-exos regulate the expression level of cytokines in vitro and in vivo. (a) Analyzed culture medium using CBA, TAxI-exos reduces the secretion of IL-2, IFN-γ and IL-17. (b) Within mice serum, using CBA and ELISA, TAxI-exos reduced the secretion of IL1-β,IL-6,TNF, while enhanced the

secretion of TGF-β, IL-4, IL-10. (C) qRT-PCR was used with spinal cords ,UMSC-exos and TAxI-exos enhanced the secretion of IL-6, IL-10, IDO-1, TNF-α.*p < 0.05, **p < 0.01, ***p < 0.001.

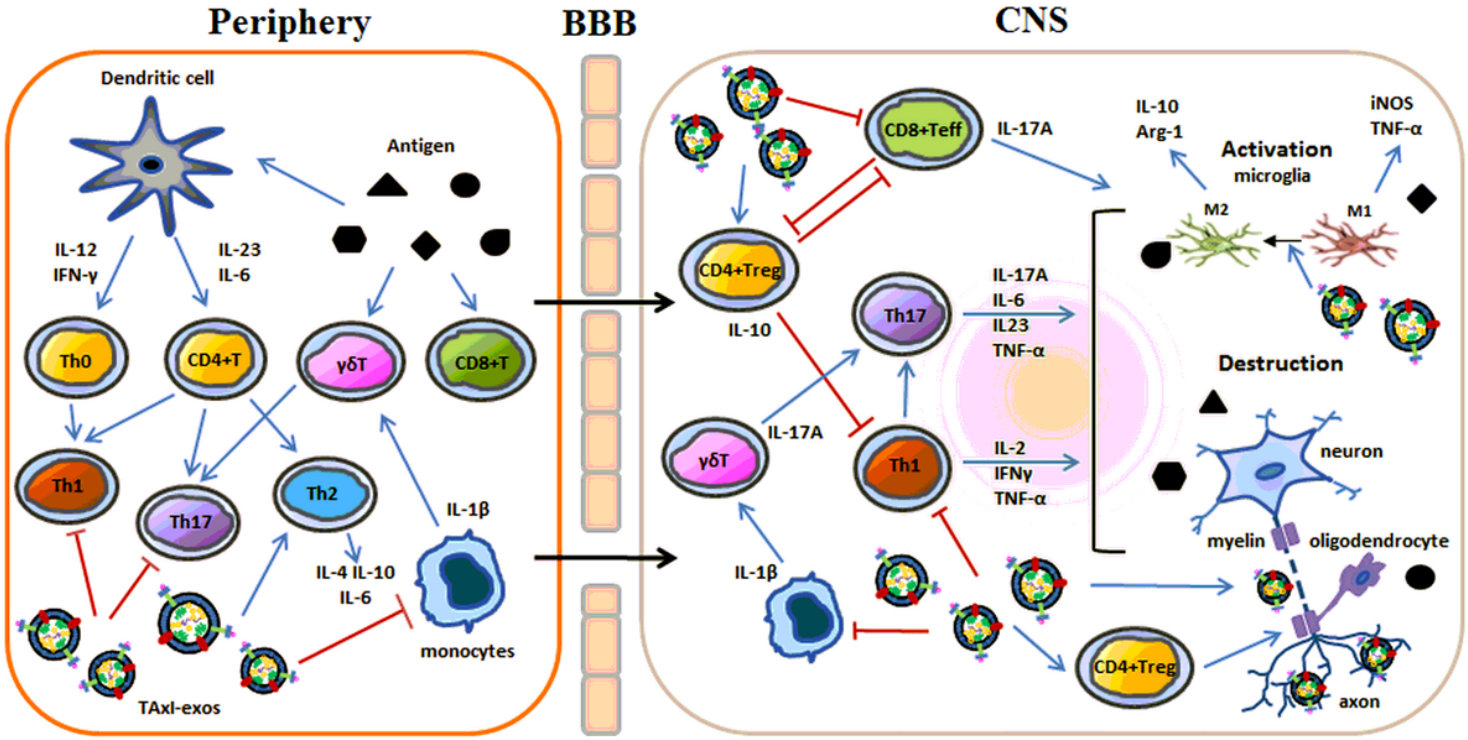

Figure 10

Diagram of major cellular and molecular mechanisms.

Supplementary Files

This is a list of supplementary files associated with this preprint. Click to download.

- SupplementaryfileforWB.pptx